1963

Vibration of an inflatable fabric wing model

Donald Dwight Seath
Iowa State University

VIBRATION OF AN INFLATABLE FABRIC WING MODEL

by

Donald Dwight Seath

A Dissertation Submitted to the
Graduate Faculty in Partial Fulfillment of
The Requirements for the Degree of
DOCTOR OF PHILOSOPHY

Major Subjects: Aerospace Engineering
Nuclear Engineering

Approved:

Signature was redacted for privacy.

In Charge of Major Work

Signature was redacted for privacy.

Heads of Major Departments

Signature was redacted for privacy.

Dean of Graduate College

Iowa State University
Of Science and Technology
Ames, Iowa

1963

TABLE OF CONTENTS

I. INTRODUCTION

A. Historical Background

At the present time there is a considerable amount of interest in inflatable space structures and winged reentry vehicles that can be packaged in small containers for the launching operation and expanded when outside the earth's atmosphere. The inflatable winged, or glider type, reentry vehicle is of particular interest for two reasons. First, the stability problems associated with boosting a large winged glider into orbit are eliminated because of the packageability of the inflatable structure. Second, the heating effect associated with reentry is reduced due to the lower wing loading provided by the increased size of the inflatable reentry vehicles.

In the past, many inflatable structures, notably balloons and airships, were made of fabric materials. More recently, the structural use of inflatable fabrics has been extended to airplanes and gliders. For use in such structures, Goodyear Aircraft Corporation has developed an inflatable platelike fabric which is called airmat. A description of airmat is presented in section II.

There have been several interesting investigations concerning platelike fabric structures and their uses for space

and reentry vehicles. Leonard et al. (18) studied collapse-loads and developed an analytical theory for the stress and deflection in inflatable fabric structures with particular application to platelike structures, such as could be used for reentry vehicles. McComb (24) developed a linear theory for inflatable plates of arbitrary shape, and Stroud (33) compared the results obtained through application of this theory with the experimentally determined deflections and natural frequencies of vibration for a square airmat plate with pinned and fixed boundaries. The comparison indicates good agreement between theoretical and experimental values and shows that for the higher modes of vibration the transverse shear stiffness is the major contributor to the plate's stiffness. For an inflatable airmat plate, the transverse shear stiffness is simply ph, where p is the internal gauge pressure and h is the plate thickness.

From model tests Zender and Deaton (40) determined the stiffness properties of a nylon-neoprene fabric material subjected to uniaxial, biaxial, or shear stresses. These stiffness properties are applicable to problems involving loads applied after the fabric is inflated.

The highly swept, delta planform design of the wing model used for this investigation was chosen because of its similarity to the planform for a reentry vehicle. Among the problems that are of interest concerning reentry vehicles is

that of aeroelastic flutter analysis, and a knowledge of the natural free vibration characteristics of a system is necessary before studying the associated flutter phenomenon.

The natural frequencies and mode shapes of a system can be found either experimentally or through the exact or approximate solution of equations which mathematically represent the system. McComb (24) developed a linear, small-deflection theory for the elastic behavior of inflatable plates. His theory, however, does not include the added stiffness effects due to the curved edges of the wing or wing model, which, particularly at low internal pressures, have a noticeable effect upon the behavior of the structure.

Influence coefficients, either computed or measured, have been used successfully for finding approximate static deflections and vibrational characteristics of many types of elastic structures. As far as the author has been able to determine from the available literature, influence coefficients have not been used previously to study the behavior of inflatable fabric wings. This paper is concerned with an experimental investigation of the vibrational characteristics of an inflatable wing model. The resonant frequencies and mode shapes are determined both experimentally and through the use of measured influence coefficients.

B. Symbols

A_{11}, A_{12}, A_{21}, A_{22}, A_{33}	- orthotropic elastic constants defined in Equations 31
a, b	- length of rectangular plate in x- and y-directions, respectively
$B_i^{(r)}$	- equals $M_i W_i^{(r)}$
C_{ij}	- element of flexibility influence coefficient matrix
D_{ij}	- element of dynamic matrix as defined in Equation 2
$E_W t$	- extensional stiffness in warp direction
$E_F t$	- extensional stiffness in fill direction
f	- frequency in cycles per second (cps)
Gt	- shear stiffness
h	- plate depth
k_{ij}	- elastic coupling term between generalized coordinates
$K_{ij}^{(r)}$	- sweeping constant derived from r^{th} mode
M_i	- element of diagonal matrix of lumped masses
M_x, M_y, M_{xy}	- plate moment resultants
m, n	- numbers of half waves in x- and y-directions, respectively
m_{ij}	- inertial coupling terms between generalized coordinates
N_{ij}	- element of column matrix as defined in Equation 15

P	- internal pressure
Q_i	- generalized force
q	- external distributed load in z-direction
q_i	- generalized coordinate
$\bar{q}_i$	- amplitude of q_i
S	- surface of the wing
$S_{ij}^{(r)}$	- element of matrix for sweeping r^{th} mode
T	- kinetic energy
U	- potential energy
$W_{ij}^{(r)}$	- ordinate to the mode shape for the r^{th} mode
w	- displacement in the z direction
x, y, z	- rectangular Cartesian coordinate system
α, β	- angles of rotation of the drop cords in the xz- and yz-planes, respectively, from their initial position normal to the xy-plane
γ_i	- assumed displacement function
ϵ, λ	- distance between grid lines in the x- and y-directions, respectively
μ_{WF}	- Poisson's ratio associated with a contraction in the warp direction due to stress in the fill direction
μ_{FW}	- Poisson's ratio associated with a contraction in the fill direction due to stress in the warp direction
ρ	- mass of plate per unit middle plane area
$\varphi_{i,j}$	- denotes either w, α or β at grid intersection
ψ	- phase angle

ω - circular frequency of vibration in radians per second

Matrix notations

$[\,]$ - general matrix

$[\,]$ - diagonal matrix

$\{\,\}$ - column matrix

$[\,]^{-1}$ - inverse of $[\,]$

II. INFLATABLE WING MODEL AND SUPPORT

A. Construction

The airmat fabric used in the construction of the inflatable wing model consists of two fabric surfaces tied together with drop cords. The cords hold the surface in a nearly parallel position when the wing is inflated. There are approximately ten drop cords per inch in the spanwise direction and six drop cords per inch in the chordwise direction. Each surface consists of an inner ply of dacron airmat weave and a cover ply of plain dacron weave coated with neoprene cement to contain the inflating gas. (See Figure 1.)

The edges of the wing model were formed by cutting off the drop cords and bending the two surfaces into the form of a half cylinder. Fabric tapes were then used to splice the two ends together. The edge construction and the detailed dimensions of the airmat and tapes are shown in Figure 2. Table 1 gives the weights of the materials used.

The inflatable wing model planform was patterned after a typical glider-type, reentry vehicle. As is shown in Figure 3 the wing model was constructed in the form of a semi-span delta wing with 67.6 degrees sweepback of the leading edge and a nearly uniform thickness of three inches.

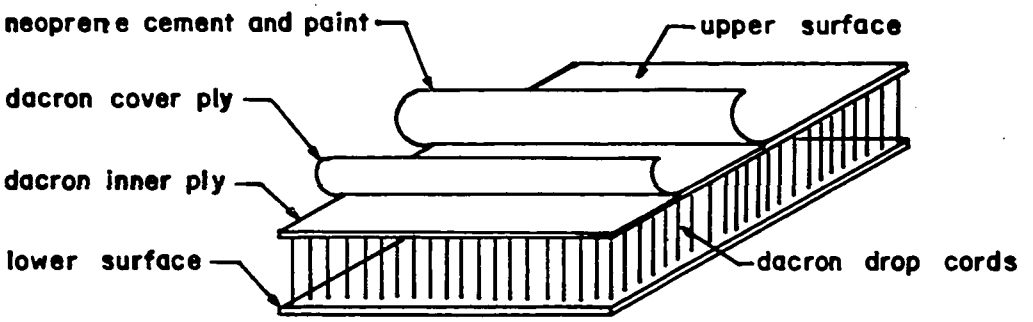

Figure 1. Airmat construction

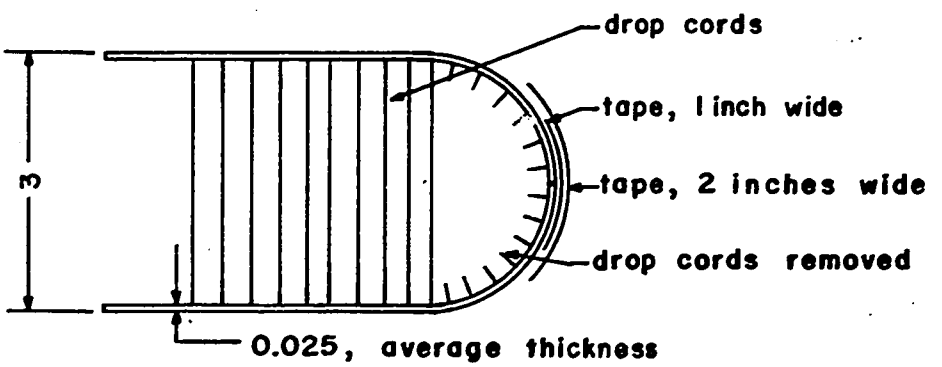

Figure 2. Wing edge construction (all dimensions in inches)

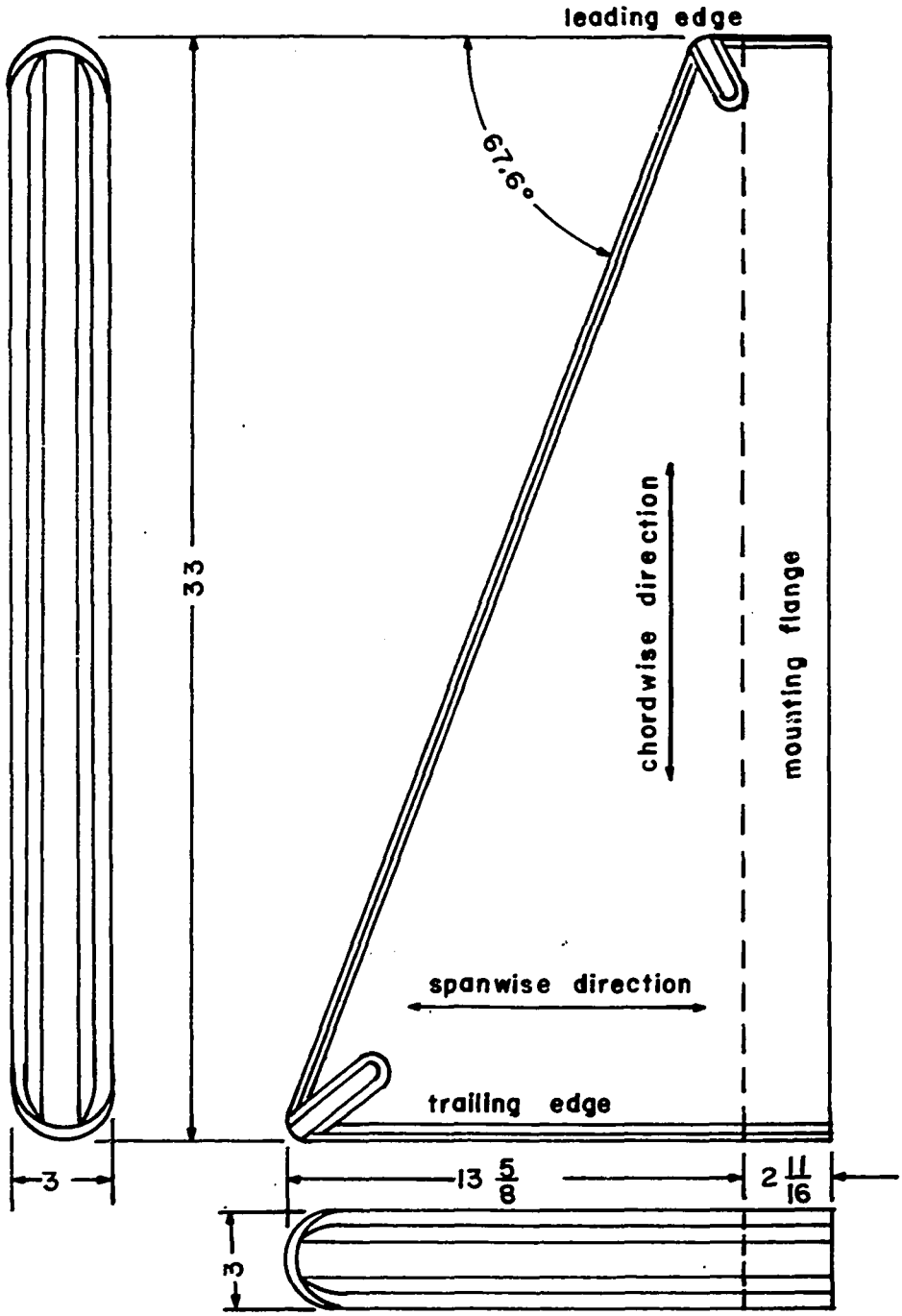

Figure 3. Inflatable wing model (all dimensions in inches)

Table 1. Material weights

Material	Weight
Airmat (including drop cords)	.002335 lb/sq in
Airmat (without drop cords)	.002024 lb/sq in
Tape - one-half inch wide	.000331 lb/in
Tape - one inch wide	.000662 lb/in
Tape - two inches wide	.001325 lb/in

The root chord and semi-span are 33 inches and 13 5/8 inches, respectively. There is a 2 11/16 inch extension at the wing root for mounting purposes. This mounting flange is merely an extension of the upper and lower surfaces with the drop cords removed. The corners of the wing model were rounded and spliced, first with one-half inch tape and then with one inch tape, and the entire wing was painted with aluminum paint.

B. Wing Support

The wing model was attached to a specially constructed steel support which was in turn attached to two large vertical I-beams embedded in a concrete footing. The flange of

the wing model was glued to the special steel support, and a one-half inch wide aluminum strip was used to bolt the flange to the support. Figure 4 shows a cross section of the wing and support, and Figure 5 shows the wing attached to the support. Steel angle irons were used to clamp the wing root at the start of the drop cords, thus giving a clamped boundary effect.

The support, in addition to holding the model, sealed the root of the wing so that the pressurizing gas could be contained, and two air inlet ports were provided.

The inflatable wing model was designed, constructed and donated by the Goodyear Aircraft Corporation of Akron, Ohio.

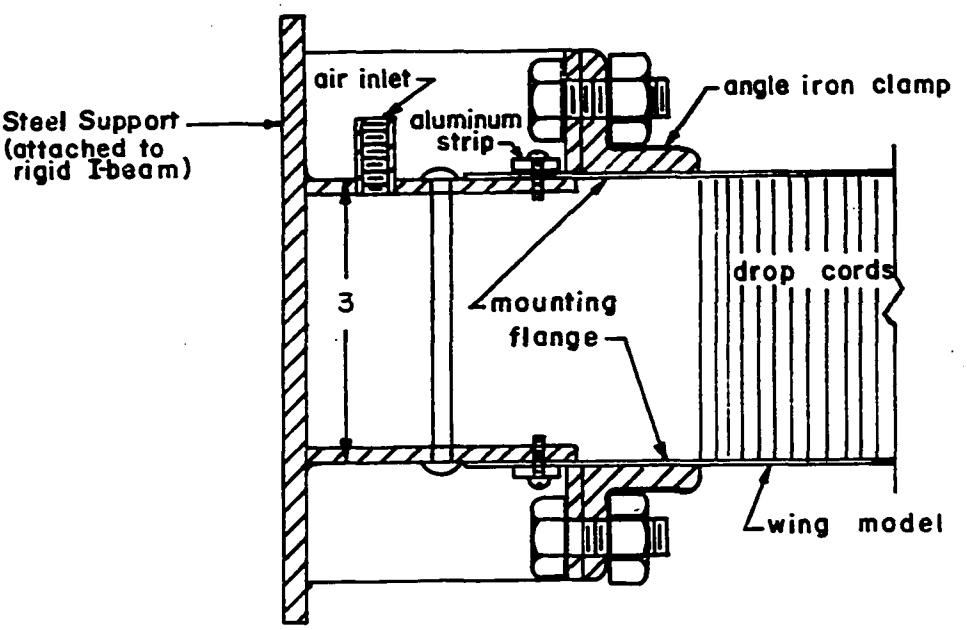

Figure 4. Cross section of wing support

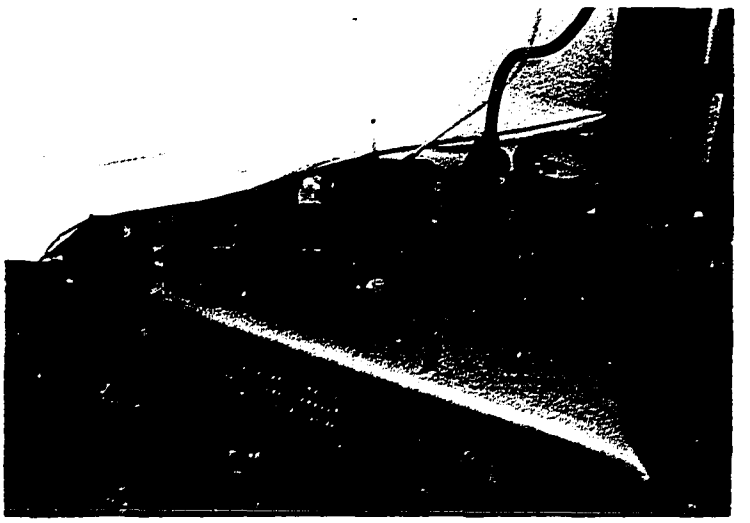

Figure 5. Wing attached to support

III. VIBRATION TESTS

The purpose of the vibration tests was to experimentally find the natural frequencies of vibration of the wing model. Figure 6 shows the vibration test setup.

A. Experimental Setup and Equipment

To find the natural frequencies it was decided to apply a sinusoidal driving force to the wing and from the response to determine the resonant frequencies. It was found that the resonant frequencies were not affected by changing the

Figure 6. Vibration test setup

position of the driving force and that only a small driving force was necessary when driving at a resonant frequency. These two facts suggested that the resonant frequencies were nearly the same as the natural frequencies.

1. Pressurizing the model

Figure 7 shows the experimental equipment used for pressurizing the model. Due to the leakage between the model and the support it was necessary to have a constant supply of pressure-controlled air entering the wing. Two regulators in series made it possible to regulate the wing pressure to within 0.02 inches of mercury. A mercury U-tube manometer was used to measure the pressure within the wing,

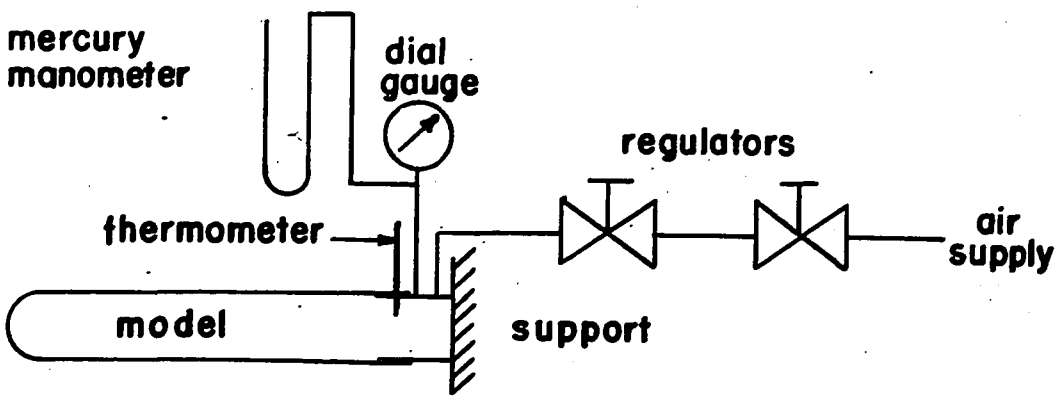

Figure 7. Schematic of pressurizing system

a dial pressure gauge was used for approximate indications of pressure, and a thermometer was used to measure the air temperature in the wing. It was found that the air temperature inside the wing was the same as the temperature of the surrounding air. A dry air supply was used to prevent contamination of the inside of the wing.

Atmospheric pressure was obtained from a mercury barometer located in the same building as the test setup. The variations in barometric pressure and temperature did not have a noticeable effect upon the test results, and therefore, average values of barometric pressure and temperature during the tests are shown with the results.

2. Exciting force

Many methods have been used to excite vibrations in a body. Electromagnets have been used extensively in research studies to excite small bodies that contain a magnetic material. Other methods include air-jet shakers (Stroud, 33), motor driven eccentrics, and rods connected to loudspeaker coils.

The inflatable wing model to be tested contained no magnetic material and therefore could not be driven by an electromagnet unless a magnetic material were externally attached to the model. However, this would probably have

altered the resonant frequencies, as would the application of the motor driven eccentric or rod connected to loudspeaker.

Mr. James Rice, of Goodyear Aircraft Corporation, suggested that the use of an ordinary loudspeaker located close to the wing might provide an adequate shaking force. This method was tried and proved to be successful; thus it was used in the test.

A twelve-inch diameter, 25-watt loudspeaker was used to excite the wing. The variable frequency sinusoidal signal obtained from a Hewlett-Packard model 202A function generator and amplified by a Knight 75-watt model KN-3076 booster amplifier was used to drive the speaker. Figure 8 shows the wiring diagram. It was found that this combination furnished more than sufficient power to excite the wing in all tests performed. The speaker, however, was modified by covering the face with a circular sheet of plywood with a $2\frac{1}{2}$ inch

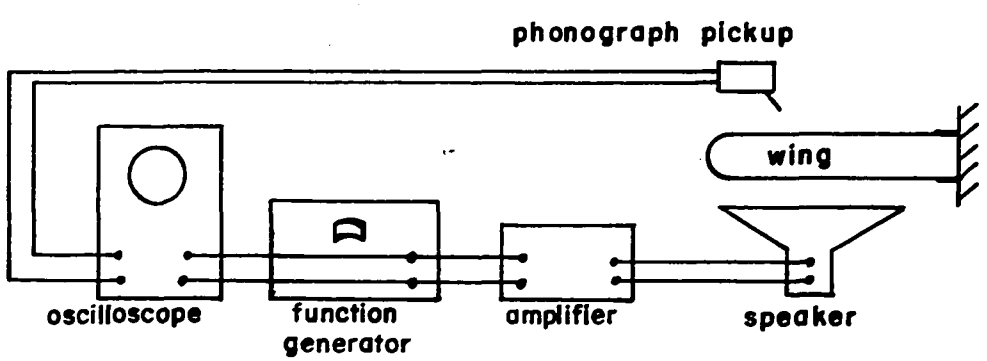

Figure 8. Wiring diagram

diameter hole in the center. This restricted the driving force to a smaller area and made it easier to determine the effect of the driving force position on the resonant frequency. The speaker was positioned approximately one-half inch from the lower surface of the wing.

3. Response detection

A Dumont type 304-A oscilloscope was used in combination with a phonograph pickup to detect the frequencies at which the wing would resonate. The phonograph pickup was placed so that the needle just touched the wing surface. Then the output signal from the needle was impressed on the vertical sweep of the oscilloscope and the signal from the function generator was impressed on the horizontal sweep of the oscilloscope. Thus, it was possible to "beat" the frequency at which the wing was vibrating against the forcing frequency. When driven at any frequency other than a resonant one, the wing vibrated with a very low response amplitude. However, at resonance all parts of the wing seemed to vibrate strongly at the resonant frequency. This enhanced response was indicated by an increase in the vertical amplitude on the oscilloscope trace.

The closest possible estimate of the natural frequency was determined in each case by reducing the power input to

the speaker to the lowest value at which vibration could be observed and at the same time carefully adjusting the function generator frequency to give maximum response as observed on the oscilloscope. It was possible to read the function generator dial to the nearest 0.1 cps for frequencies up to 120 cps and to the nearest 1.0 cps for frequencies above 120 cps.

4. Calibration of the function generator

The function generator was calibrated against a Hewlett-Packard Model 522B electronic counter at the beginning and end of a three-month period during which the wing model was tested. Comparing the two calibrations, it was found that the maximum frequency variation was less than one per cent over the range of frequencies needed for the wing vibration tests.

The operating manual for the function generator specified a frequency stability of one per cent. This meant that the readings for the experimental resonant frequencies were subject to this one per cent error. Specifications for the electronic counter stated that it was accurate to within one count, which for the time interval used for counting gave an accuracy to within 0.1 cps. It was also found that the function generator required approximately one hour of warmup

time to stabilize. Therefore, a warmup time of at least one hour was allowed before any experimental frequencies were measured.

5. Air-jet shaker

In addition to the speaker-shaker arrangement described above, an air-jet shaker (Herr, 12) was constructed and used to excite the wing model. A schematic of the shaker is shown in Figure 9, and photographs of the shaker are shown in Figures 10 and 11.

Air-jets approximately one-eighth of an inch in diameter were positioned so that one impinged perpendicularly on the lower wing surface and the other on the upper surface. Pressurized air was supplied to the jets through an adjustable pressure regulator and hoses. Two interrupter discs attached to a shaft were placed between the jets and the wing as shown in the figure. When the shaft rotated, the discs would alternately pulsate the two airstreams so that they impinged on the upper and lower surfaces 180 degrees out of phase. The interrupter used produced a square wave forcing function. A sinusoidal wave could have been obtained by using a different shape for the interrupter discs.

The motor used for turning the shaft carrying the two discs was a 28-volt d.c. shunt motor for which the speed

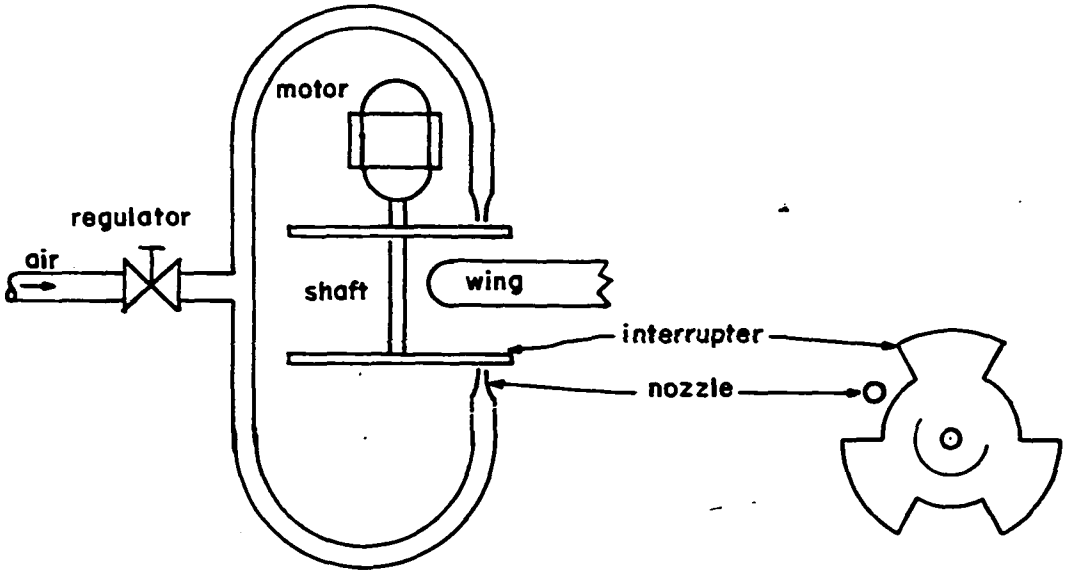

Figure 9. Sketch of air-jet shaker

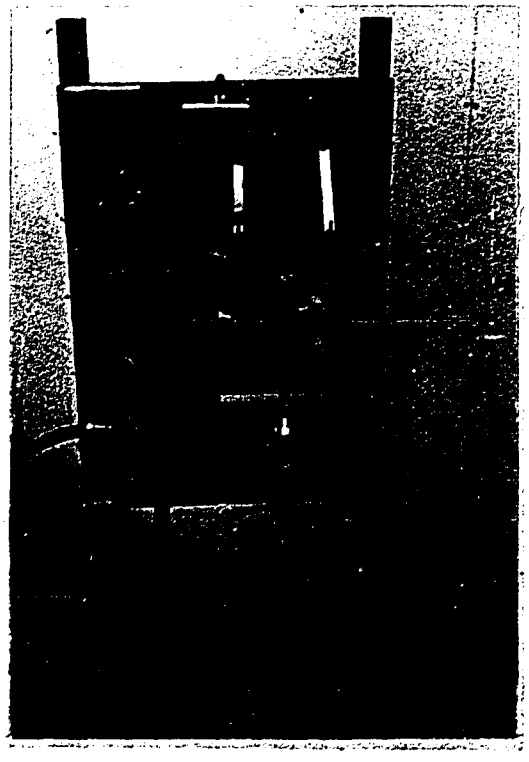

Figure 10. Air-jet shaker

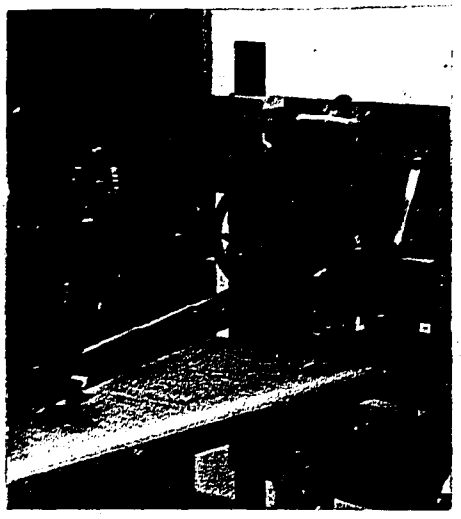

Figure 11. Air-jet shaker and wing model

could be varied by means of a rheostat in series with the armature circuit. It was found that with this speed arrangement, the shaker could be controlled to within two cps for the range of frequencies from 45 cps to 180 cps.

As was done with the speaker-shaker arrangement, the function generator signal was used to "beat" against the wing response to measure the resonant frequencies. Due to the structural limitations on the shaker, only the first five modes of vibration were measured. This was done for internal wing pressures of three, five, seven and nine psig.

Another limitation of the air-jet shaker was that it could be used only near the edge of the structure. However, the use of discs with larger diameters would permit moving the jets farther inward from the edge.

B. Experimental Results

1. Experimental resonant frequencies

The measured experimental resonant frequencies excited by the speaker shaker are shown in Figure 12. These are accurate to within 1 per cent, the limiting accuracy figure of the function generator. Figure 13 shows the experimental resonant frequencies excited by the air-jet shaker.

Experimental Resonant Frequencies, cps							
Mode	Wing Internal Pressure, psig						
	3	4	5	6	7	8	9
1	49.1	53.7	55.9	58.4	61.3	63.2	65.1
2	75.7	86.1	95.2	103.2	108.6	113.5	118
3	88.6	98.0	105.8	112	116	120	127
4	98.3	113	123	133	143	150	157
5	105.9	124	136	148	160	169	176
6	115.5	138	153	170	184	195	206
7	128	149	164	181	195	206	218
8	148	168	183	199	213	226	238

Average Barometric Pressure = 29.00 in. Hg

Average Temperature = 73° F

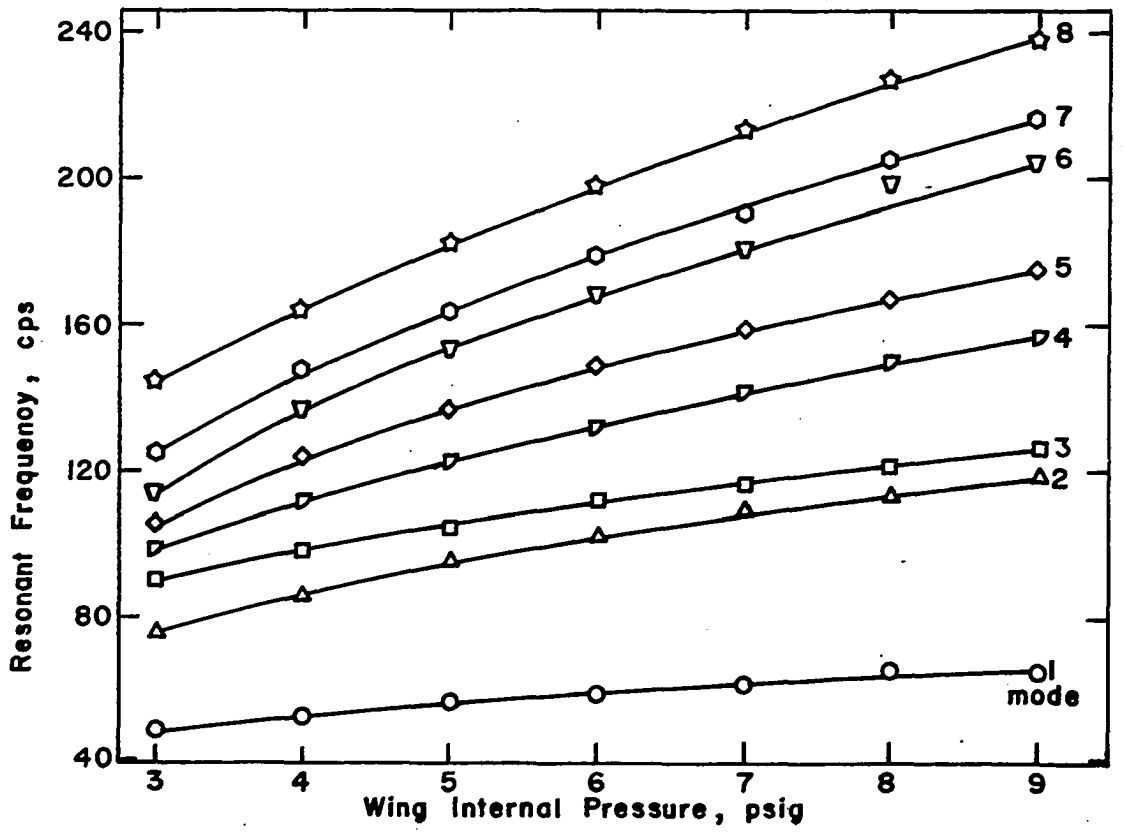

Figure 12. Experimental resonant frequencies of vibration excited with speaker shaker

Experimental Resonant Frequencies, cps				
Mode	Wing Internal Pressure, psig			
	3	5	7	9
1	49.0	56.3	61.3	65.2
2	75.1	95.6	109.6	117
3	89.6	105.7	117	128
4	97.5	122	144	160
5	103.7	137	160	176

Average Barometric Pressure = 29.00 in. Hg
Average Temperature = 73° F

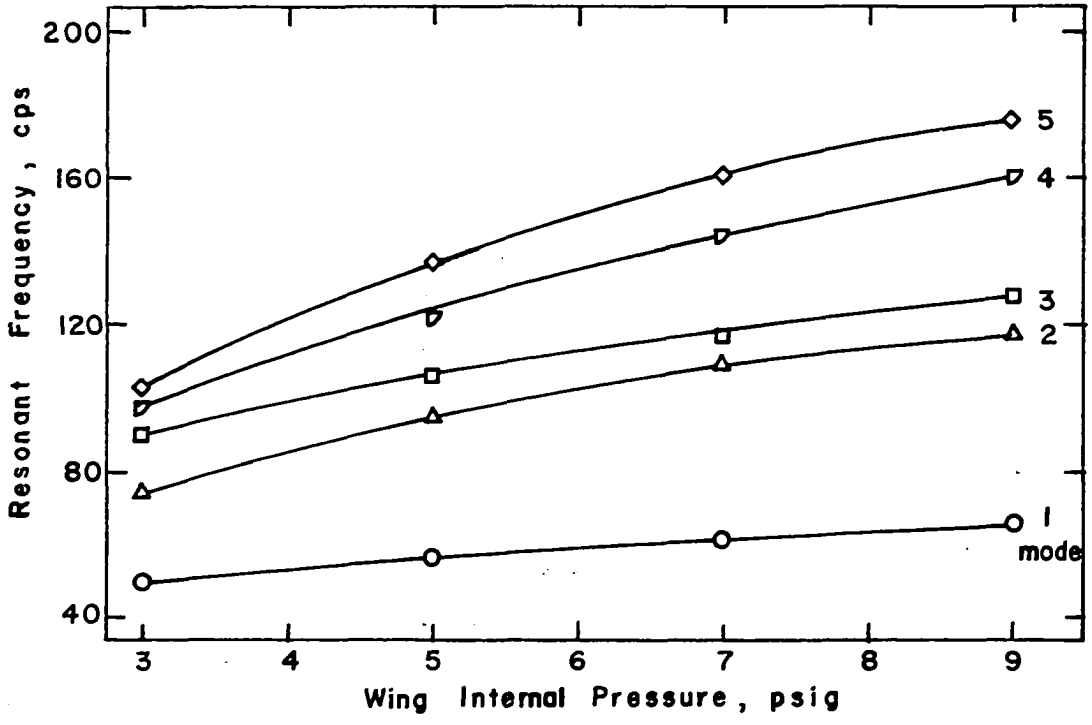

Figure 13. Experimental resonant frequencies of vibration excited with air-jet shaker

2. Mode shapes

Figures 14 through 17 show the nodal patterns for the lowest eight modes of vibration for internal wing pressures of 3, 5, 7 and 9 psig. Pictures were also made for pressures of 4, 6 and 8 psig, but are not included because they do not show any significant differences from those which are included. In some cases in order to form the nodal patterns it was necessary to move the driving force to avoid driving directly on a nodal line. Whole poppy seeds were used to form the nodal patterns because their color contrasted to that of the wing.

Several statements can be made concerning the experimental resonant frequencies.

(a) The horizontal position of the driving force had no noticeable effect on the resonant frequency unless the driver was positioned near the leading edge of the root chord of the model (sections 5 and 10 as indicated in Figure 18). Then the resonant frequency showed an increase of as much as 1 per cent.

(b) The distance between the speaker-shaker and the lower surface of the wing had no noticeable effect on the resonant frequency except when the distance became less than 1/2 inch. Then the resonant frequency was lowered. This could be caused by increased damping produced when the

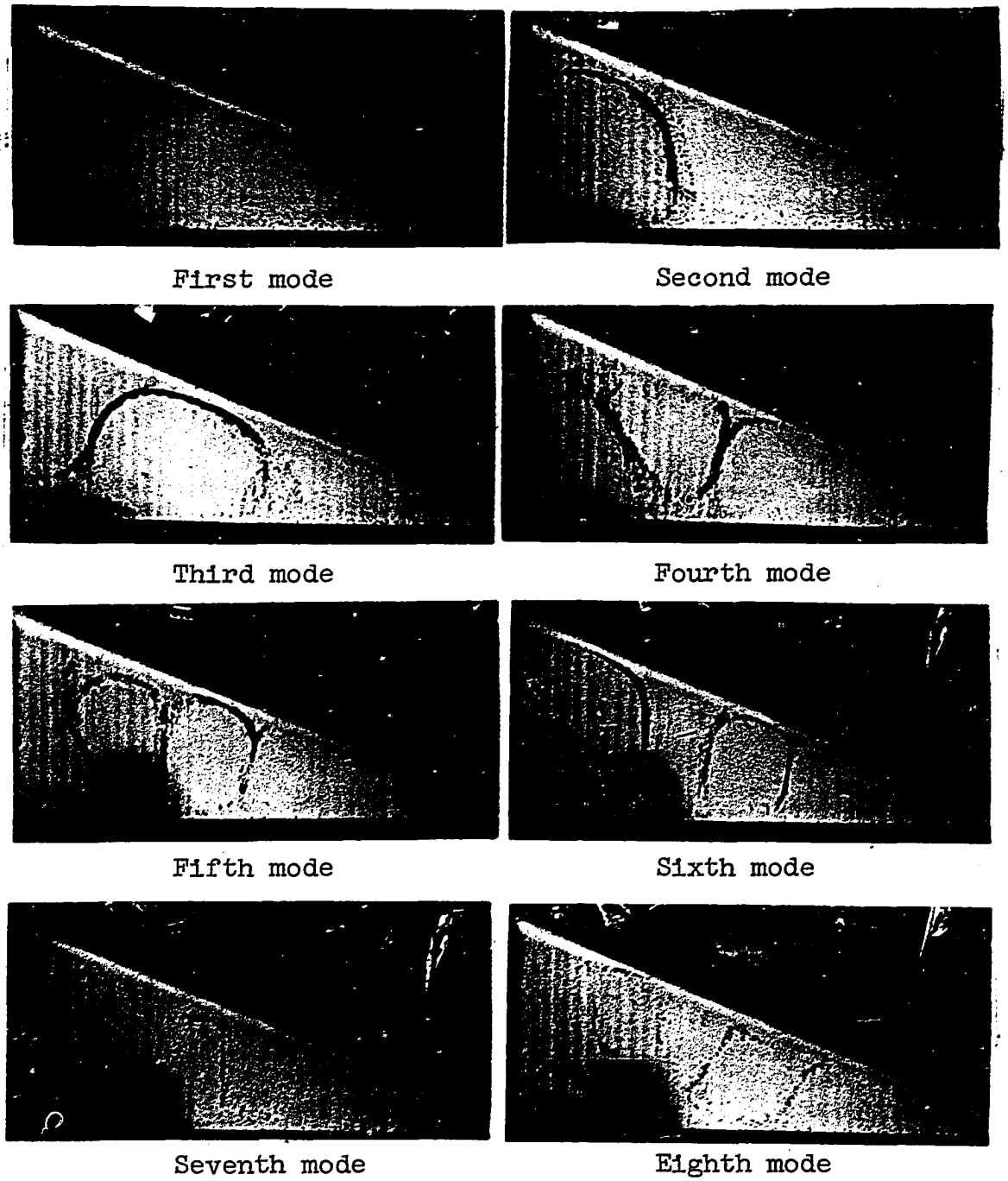

Figure 14. First eight nodal patterns for three psig internal wing pressure

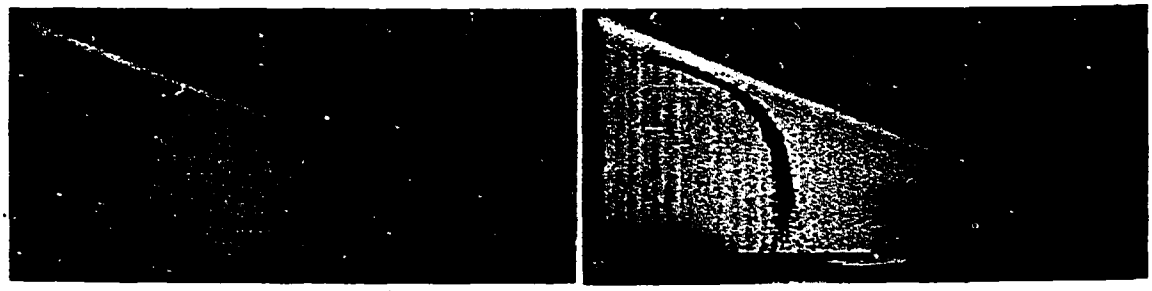

First mode

Second mode

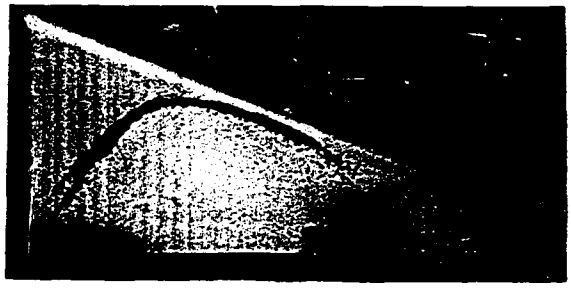

Third mode

Fourth mode

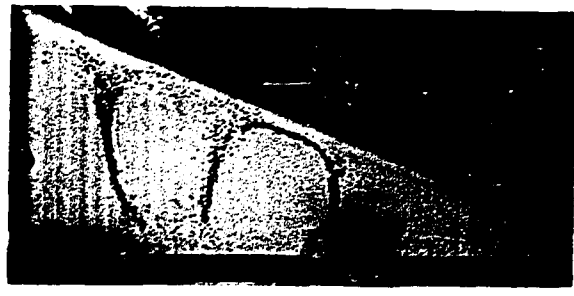

Fifth mode

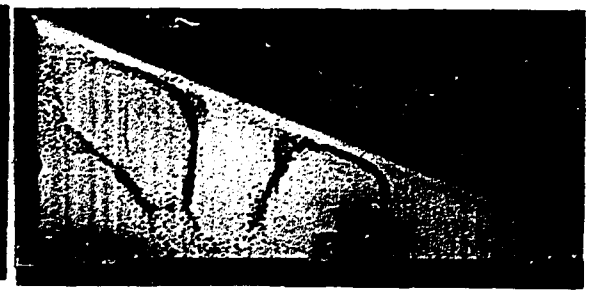

Sixth mode

Seventh mode

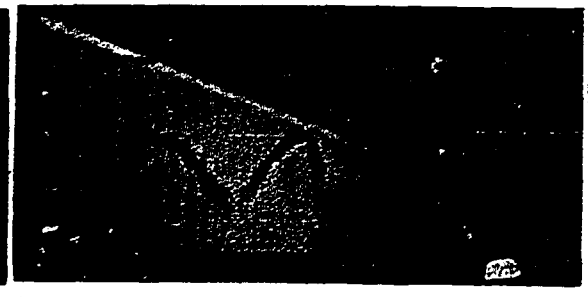

Eighth mode

Figure 15. First eight nodal patterns for five psig internal wing pressure

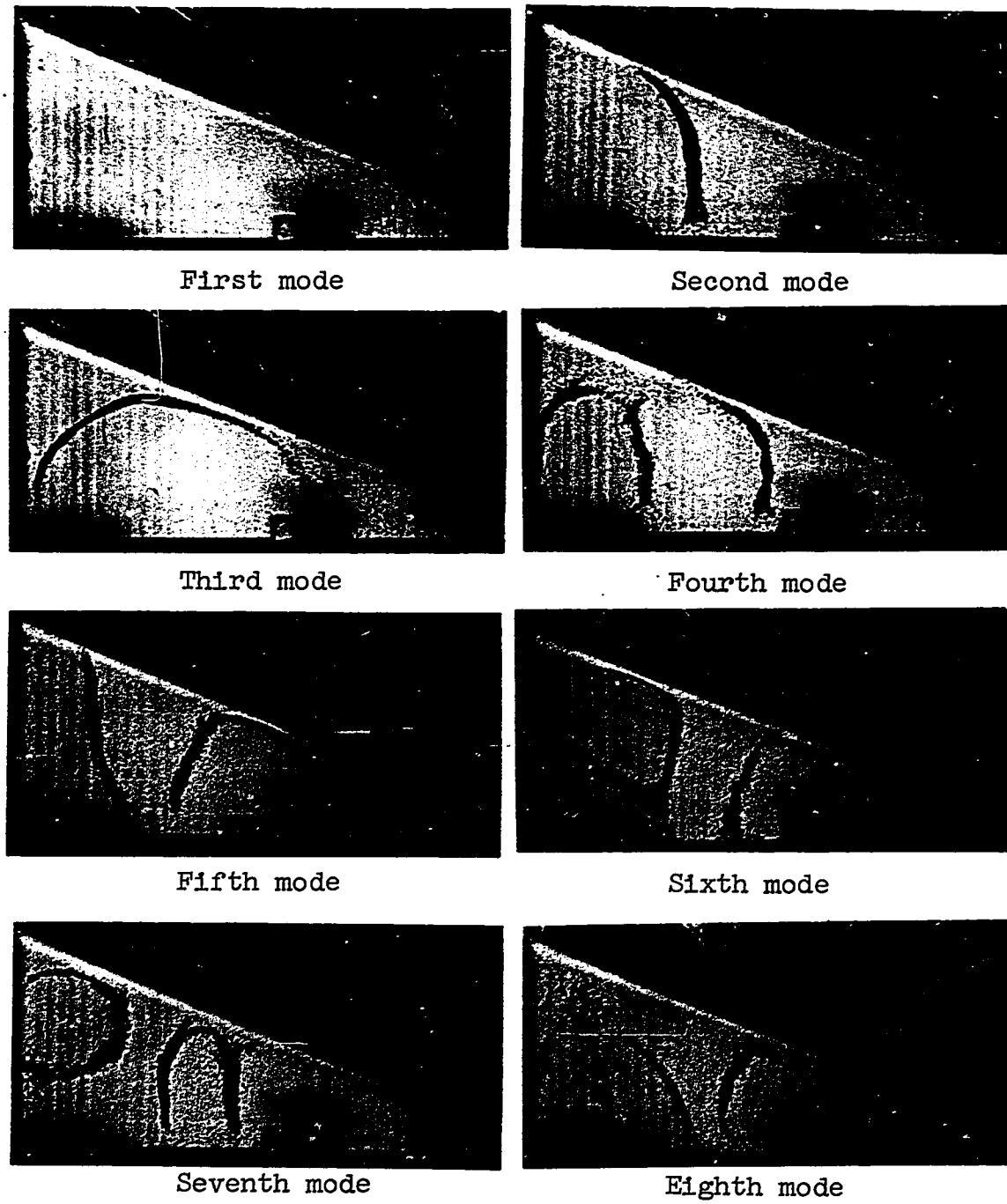

Figure 16. First eight nodal patterns for seven psig internal wing pressure

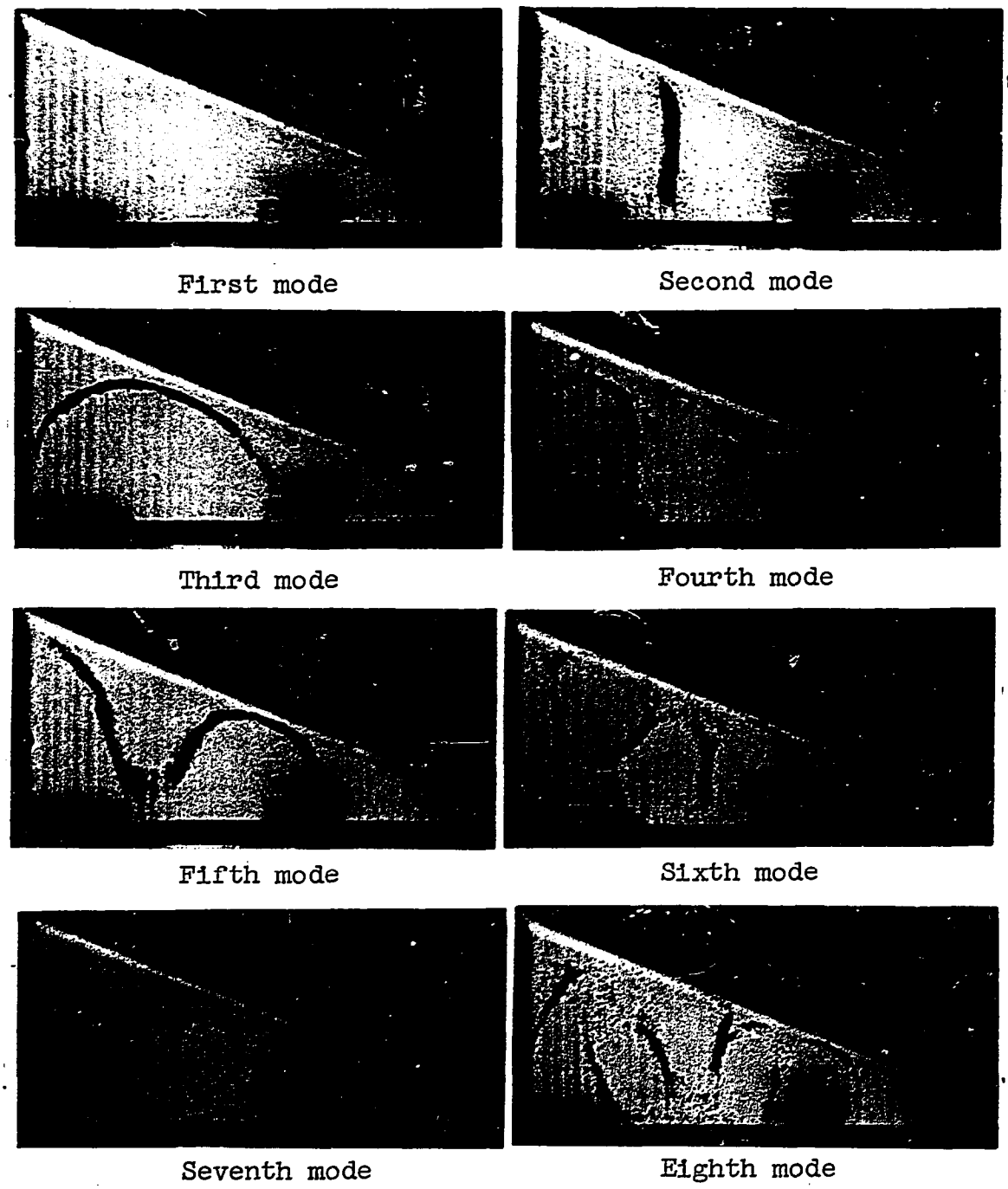

Figure 17. First eight nodal patterns for nine psig internal wing pressure

pulsating air flow from the speaker shaker is not able to escape and re-enter quickly enough through the reduced region between the speaker and the wing model. The presence of this "trapped" air increases the effective damping of the system and thereby reduces the resonant frequency of vibration.

(c) When the wing was excited in the first mode, the resonant frequency dropped approximately 1 per cent as the amplitude of the driving force was increased by a factor of ten. The reason for this could be the same as that given for (b). An increase in amplitude of the speaker shaker causes an increase in the amount of air that must escape and re-enter between the speaker and the wing model in a given length of time. This effectively increases the damping of the system and lowers the resonant frequency.

(d) The position of the phonograph pickup, either on the wing model surface or on the root support, showed no measurable change in the resonant frequency.

IV. INFLUENCE COEFFICIENT METHOD

One method of finding the natural frequencies of vibration with small deflections, as described in Bisplinghoff et al. (3), is that using lumped masses and flexibility-influence coefficients. In this method the wing is divided into sections, and the mass of each section is assumed concentrated at its center of gravity, so that the wing is replaced by a weightless system carrying the lumped masses at discrete stations.

The matrix equation representing the wing is

$$\frac{1}{\omega^2} \{W\} = [D]\{W\}, \qquad \text{(Eq. 1)}$$

where

$$[D] = [C][M]; \qquad \text{(Eq. 2)}$$

ω is the natural circular frequency, the elements of the column matrix $\{W\}$ are the ordinates of the mode shape, the elements of the square symmetric matrix $[C]$ are the influence coefficients C_{ij} (the deflection at the i^{th} station due to a unit load at the j^{th} station), and the elements of the diagonal matrix $[M]$ are the section masses. In Equation 1, derived in Appendix A, only the transverse deflections of

the wing are considered. Ordinarily the accuracy of this method is increased as the number of sections is increased.

A. Lumped Masses

In order to substantiate the theory that accuracy increases as the number of sections increases, the wing was first divided into ten sections as shown in Figure 18, and then it was divided into eighteen sections as shown in Figure 19. The wing model section masses and center of gravity locations are also shown in the figures. These are the masses of the model fabrics only and do not include the mass of the pressurized internal air.

However, before using these section masses in Equation 2, the mass of the internal air, which depends upon the temperature and absolute pressure inside the wing, must be added. The mass of the internal air was computed using 29.00 inches of mercury for an average value of barometric pressure and 73 degrees Fahrenheit for an average value of temperature inside the wing. The use of these average values did not introduce any appreciable errors for the operating ranges of barometric pressure and temperature observed during the tests. Appendix B shows the influence coefficient and mass matrices used for each internal wing pressure as well as the natural frequencies and mode shapes

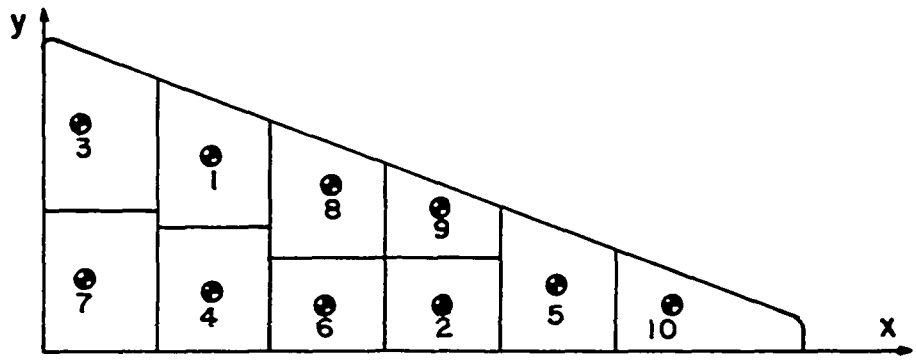

Section Number	[a] Mass $\times 10^4$ $(\frac{lb-sec^2}{in.})$	Coordinates of c.g., (in.)	
		x	y
1	2.150	7.47	8.56
2	1.219	17.50	2.00
3	2.960	1.87	9.83
4	1.510	7.50	2.50
5	1.967	22.47	2.90
6	1.210	12.50	2.50
7	2.370	1.84	3.00
8	1.900	12.47	7.06
9	1.327	17.47	6.46
10	2.090	27.26	1.90

[a] Mass of internal air is not included

Figure 18. Wing divided into ten sections

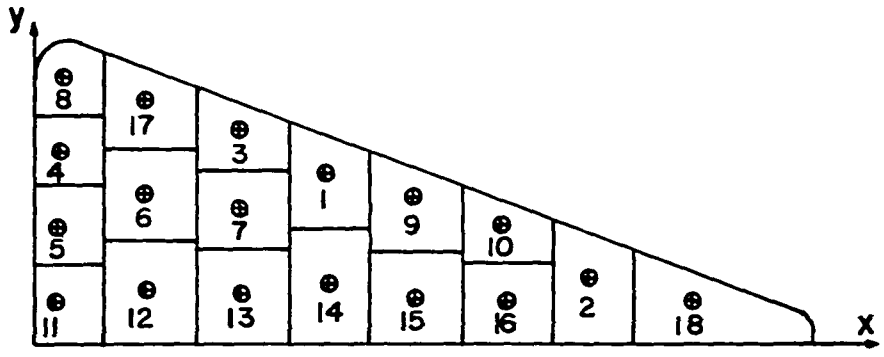

Section Number	[a] Mass $\times 10^4$ $(\frac{lb-sec^2}{in})$	Coordinates of c.g. (in.)	
		x	y
1	1.182	12.68	7.39
2	1.294	24.18	2.73
3	1.056	8.88	9.31
4	0.878	0.97	8.50
5	1.002	0.97	4.75
6	1.184	5.00	6.50
7	0.847	9.00	5.75
8	1.058	1.55	11.60
9	1.210	16.39	6.17
10	0.978	20.38	5.12
11	0.988	0.97	1.75
12	1.088	5.00	2.25
13	0.969	9.00	2.00
14	1.060	12.75	2.50
15	0.969	16.50	2.00
16	0.847	20.50	1.75
17	1.162	4.89	10.73
18	1.110	28.88	1.82

[a] Mass of internal air is not included

Figure 19. Wing divided into eighteen sections

for the first four modes of vibration which result from the matrix iteration of Equation 1.

B. Measuring Influence Coefficients

Due to the difficulty involved in computing influence coefficients, it was decided to measure them directly. In order to do this a sequence of vertical loads was applied in turn at each of the sections, and for each loading the corresponding deflection at each section, including that at the loaded section, was measured. The procedure is outlined below.

First, an initial load was applied to remove any slack in the system, and then several successive loads of at least 100-gram increments were applied and then withdrawn. For each load the displacements were measured with a Brown and Sharpe micrometer head attached to a beam which in turn was attached to the wing support. By means of a battery and light circuit that was closed when the micrometer made contact with a small copper plate attached to the surface of the wing, deflections could be measured to the nearest 0.00005 inch. (See Figure 20.)

The most satisfactory method of loading was determined by experiment. It was found that applying the load to the wing surface through a 3/8 inch sphere did not result in

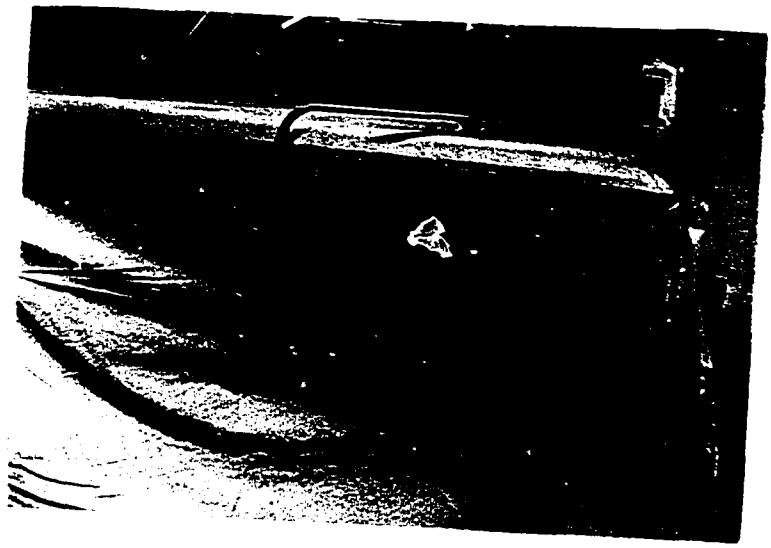

Figure 20. Measuring influence coefficients

equal deflections of the upper and lower surfaces. Hence, various sizes of 1/8 inch thick plastic plates were tried between the loading point and the wing surface, causing a distribution rather than a point application of the load. It was found that a plastic plate, one-inch square or larger, produced equal deflections of the upper and lower surfaces. Due to the large size of the wing sections when only ten subdivisions were used, a plastic plate two inches square was employed for loading. This produced a deflection that seemed to more nearly represent the average deflection of the loaded section. Whether or not a plate was used had no noticeable effect on the deflections at sections other than

the one at which the load was applied.

Total loads were kept as small as possible in an attempt to produce deflections of the same order of magnitude as those produced when the wing was excited and to minimize buckling effects of the wing surfaces. However, it was necessary to apply loads of sufficient magnitude to produce deflections large enough to reduce the errors in reading the micrometer. To do this it was necessary with each loading increment to produce an incremental deflection of at least 0.0010 inch. This resulted in errors of ten per cent or less for each deflection measurement reading. The loading weights used were checked on a balance and found to be within one per cent of their represented values. Figure 21 shows a typical load-deflection curve used for determining influence coefficients. The slope of the visually fitted line shown is 0.008615 in/lb. A least squares fit to the data points resulted in a line with a slope of 0.008602 in/lb. Because of the small difference between the slope of the visually fitted line and the slope of the least squares line, the influence coefficients used were those determined by the slope of a visually fitted line. Using this method it is believed that the measured values of the influence coefficients are not incorrect by more than two per cent.

It can be shown (Fung, 6) by the reciprocal deflection theorem that the matrix of influence coefficients is

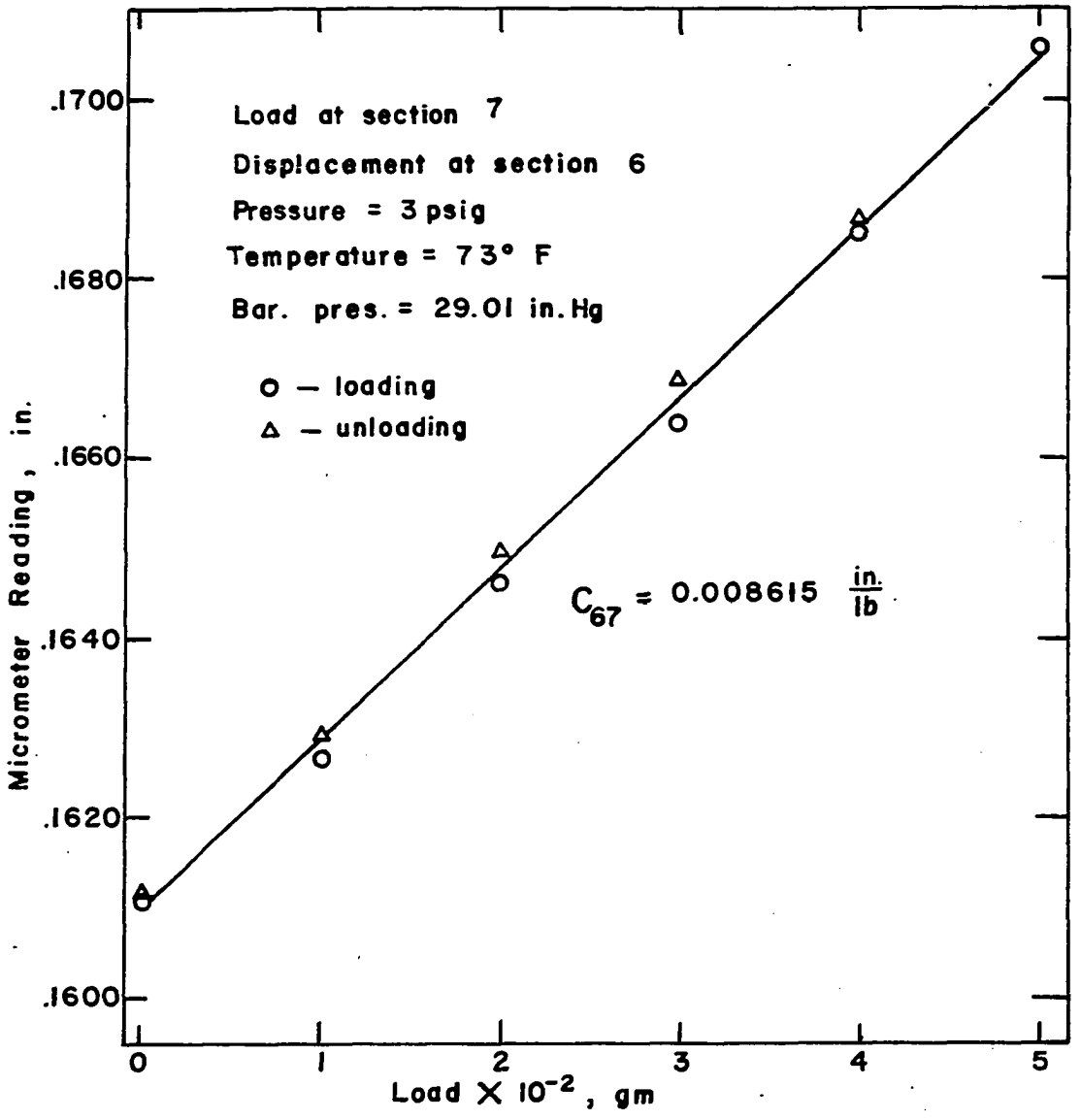

Figure 21. Typical graph of load versus displacement used for determining influence coefficients

theoretically symmetrical: i.e. $C_{ij} = C_{ji}$. However, the experimentally measured values of C_{ij} sometimes differed from the corresponding values of C_{ji} by as much as ten per cent. Therefore, the values of C_{ij} and C_{ji} were averaged to form a symmetrical matrix of influence coefficients. Appendix B shows the averaged influence coefficient matrices for wing pressures of 3, 5, 7 and 9 psig.

C. Results

Table 2 shows the natural frequencies as computed by the influence coefficient, matrix-iteration method. These are indicated for both the ten-section subdivisions and the eighteen-section subdivisions.

Iterations and sweeping operations used in finding the natural frequencies were performed with the Iowa State University Cyclone Digital Computer. The iteration process for each mode was begun with all elements of the column matrix $\{W\}$ set equal to unity, as indicated in Appendix B, and this procedure was continued until the resulting frequency from the i^{th} iteration differed from the frequency resulting from the $(i-1)^{st}$ iteration by less than 0.03 cps. Figures 22 through 26 show the resulting ordinates of the mode shapes.

Flomenhoft (5) pointed out the possibility of iteration

Table 2. Natural frequencies by influence coefficient method, cps

Mode	Internal wing pressure, psig			
	3	5	7	9
1	47.0[a](49.1)[b]	54.3[a](55.9)[b]	59.0[a](61.3)[b] [62.6][c]	63.3[a](65.1)[b]
2	68.9[a](75.7)[b]	87.5[a](94.6)[b]	92.9[a](108.6)[b] [100.0][c]	101.9[a](122)[b]
3	72.2[a](88.6)[b]	96.6[a](105.8)[b]	107.0[a](116)[b]	117.7[a](127)[b]
4	72.2[a](98.3)[b]	93.6[a](123)[b]	107.6[a](143)[b]	119.1[a](157)[b]

[a]Using ten wing sections.

[b]Experimental value.

[c]Using eighteen wing sections.

errors in modes above the fundamental arising from small differences of large numbers which are not carried by the calculating equipment. To overcome this he advised arranging the sweeping operation so that the section with the largest product of mass times mode-ordinate would be swept out. This product is called $B_1^{(r)}$ in Appendix A. His advice was followed, and after the first mode was computed, the input data were rearranged so that the largest $B_1^{(1)}$ would be swept out when finding the second mode. After the

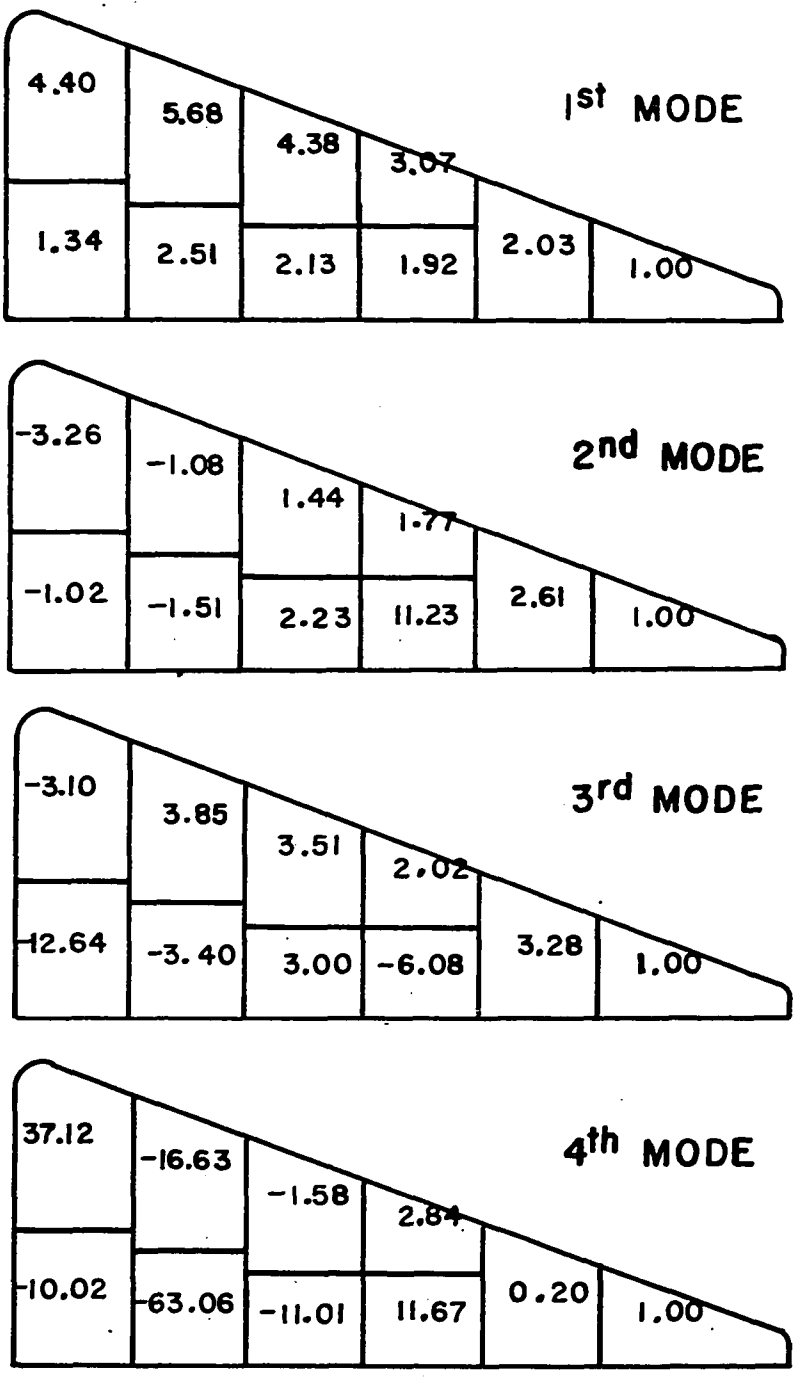

Figure 22. Ordinates of the mode shapes for the first four modes at three psig internal wing pressure using ten sections

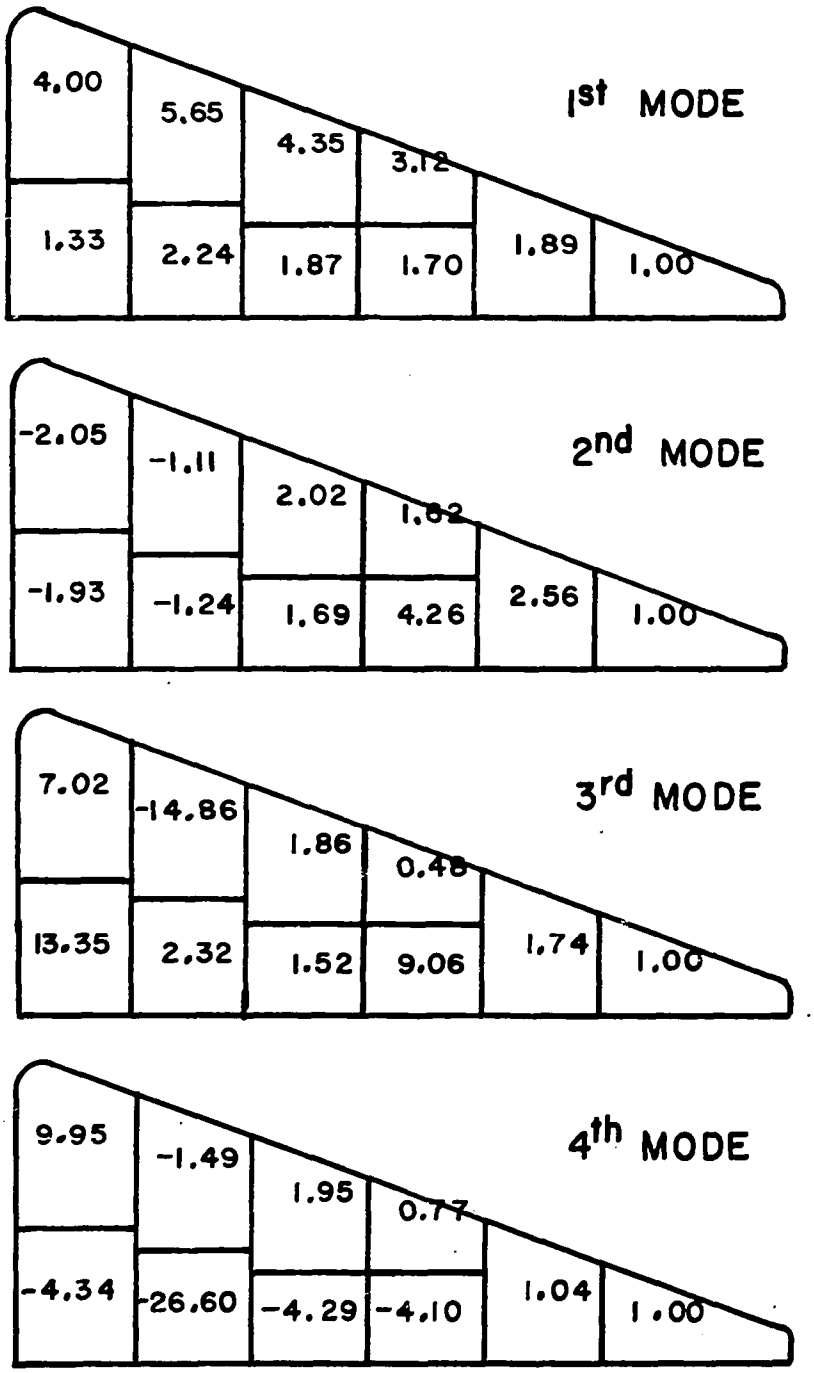

Figure 23. Ordinates of the mode shapes for the first four modes at five psig internal wing pressure using ten sections

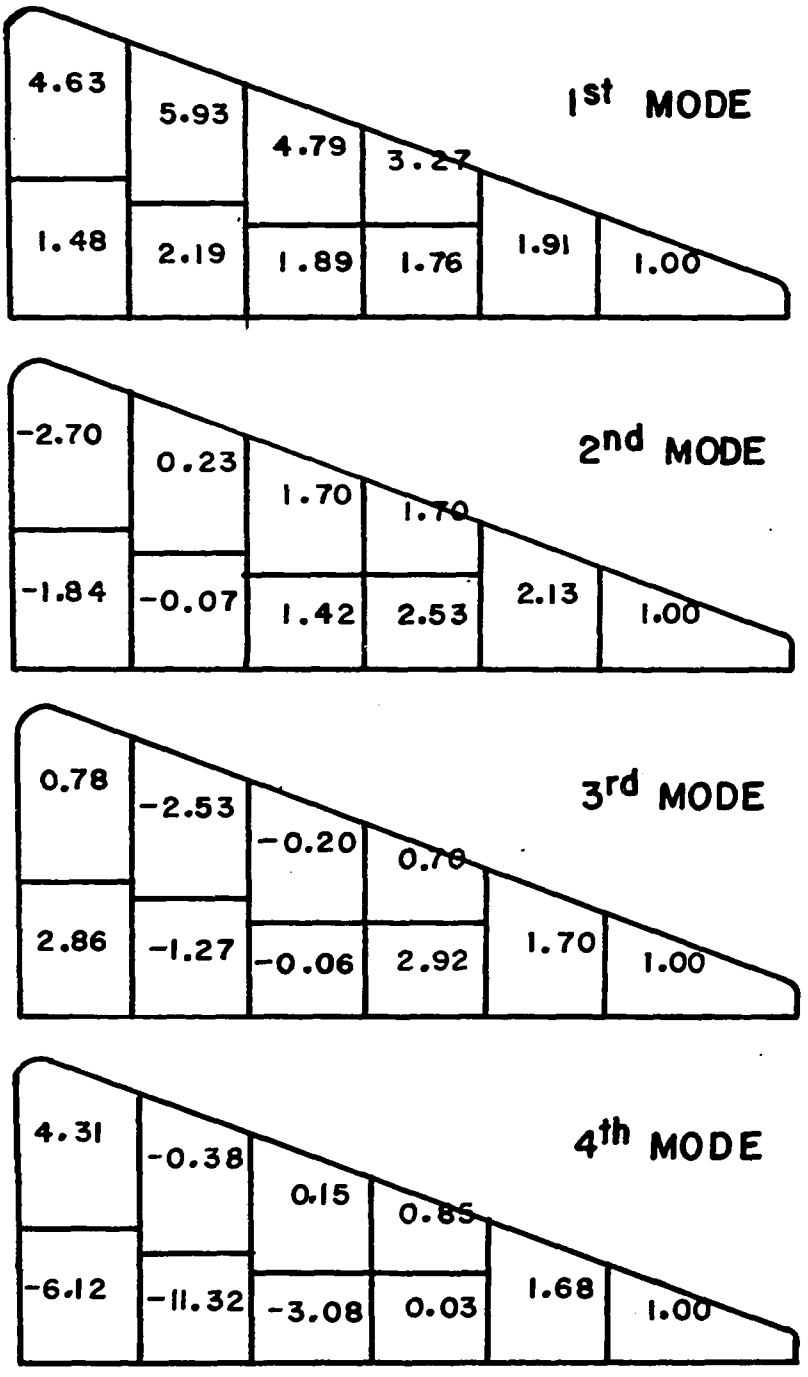

Figure 24. Ordinates of the mode shapes for the first four modes at seven psig internal wing pressure using ten sections

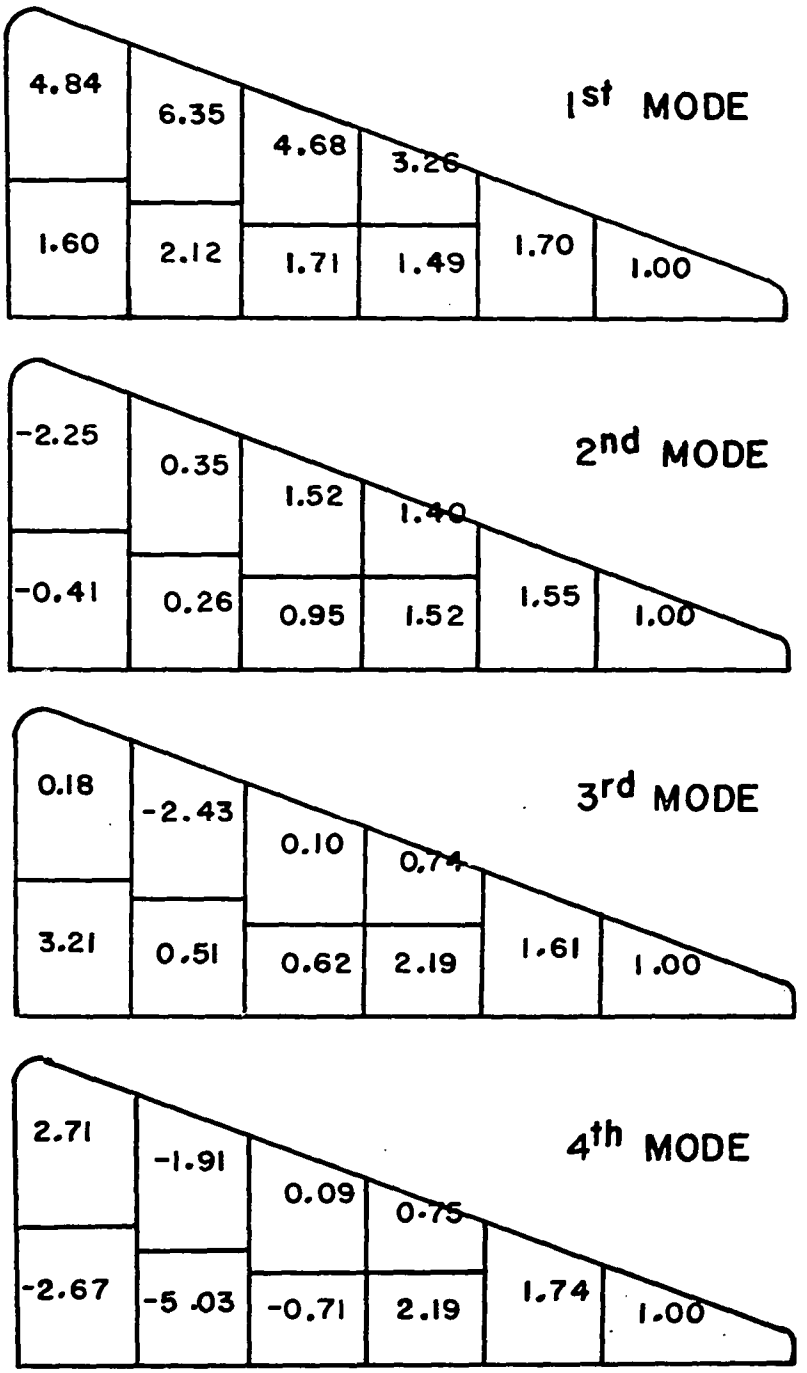

Figure 25. Ordinates of the mode shapes for the first four modes at nine psig internal wing pressure using ten sections

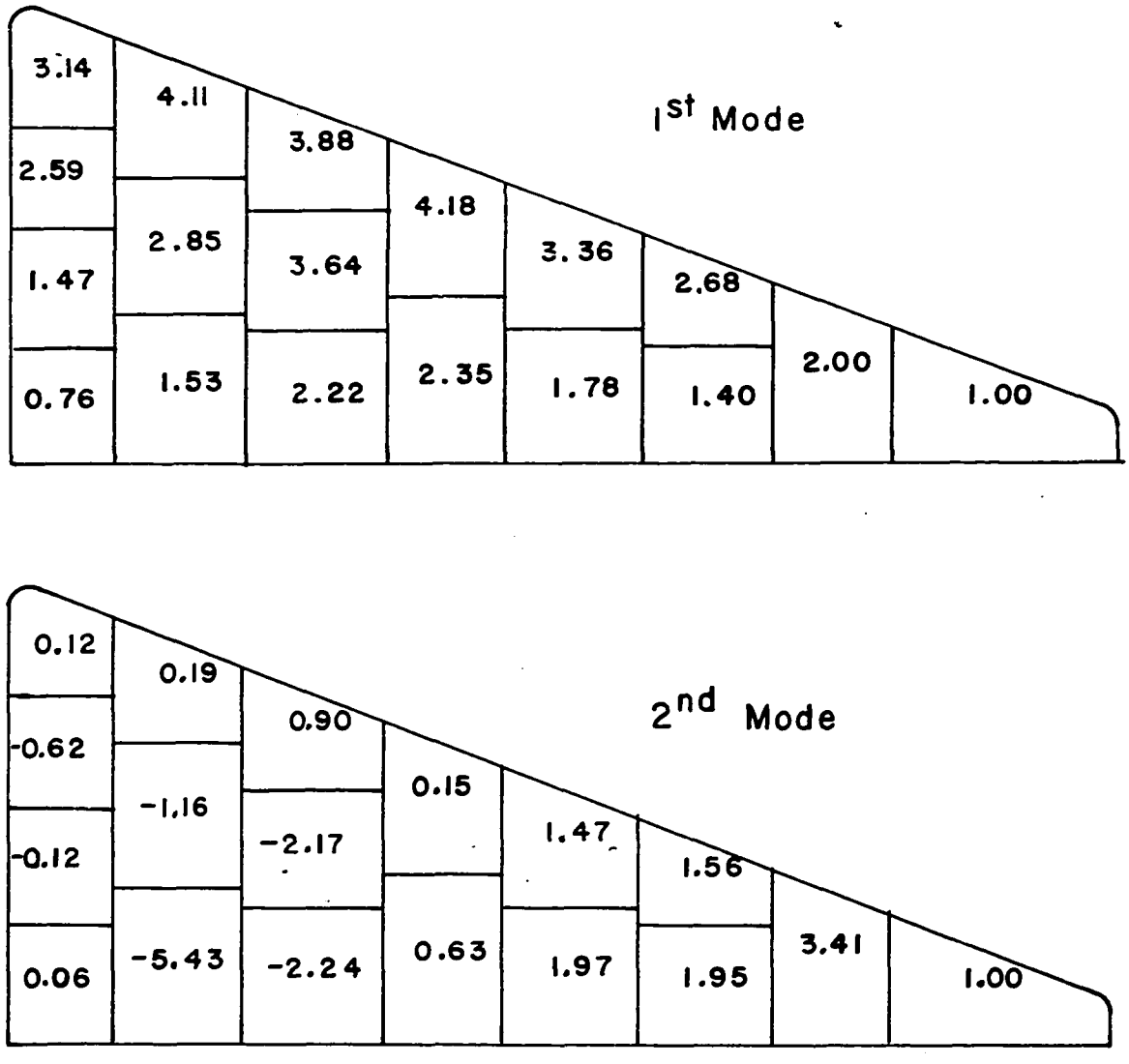

Figure 26. Ordinates of the mode shapes for the first two modes at seven psig internal wing pressure using eighteen sections

second mode was found, the data were again rearranged so that the largest remaining $B_i^{(1)}$ would be the next to be swept out. This was also done after the third mode was found. In the case where the section masses are nearly equal, the section having the largest main diagonal influence coefficient usually produces the largest $B_i^{(r)}$. Because of the above mentioned rearrangements the section numbers in Figures 18 and 19 are not in a logical sequence. Before rearrangement, the computation of the second mode for the wing divided into eighteen sections resulted in a nodal line that was nearly perpendicular to the experimentally observed position of the nodal line. After rearranging so that the sweeping operation would sweep out the largest value of $B_i^{(1)}$, the position of the nodal line agreed quite well with that determined experimentally. The effect on the natural frequency was not so drastic, changing its value by only a few per cent.

V. DISCUSSION

A. Discussion of Results

1. Experimental results

As illustrated in Figure 12, the resonant frequency for each mode increases with an increase in the gauge pressure of the air inside the wing. A graph of the experimental data on log-log graph paper (Figure 27) shows that frequency is proportional to the gauge pressure raised to the 0.216 power for the first mode, 0.427 for the second mode, 0.425 for the fourth mode and 0.430 for the eighth mode. Stroud (33) found that for the higher modes of a one-inch thick, square, inflatable plate clamped on all edges, the resonant frequency is proportional to the gauge pressure raised to the 0.500 power.

An examination of the photographs of the nodal patterns (Figures 14-17) reveals some interesting phenomena. Comparison of the patterns for the second mode as the wing internal pressure is increased shows a straightening of the nodal line in the spanwise direction and a disappearance of the line near the curved edge of the model until the vibration appears to be predominantly torsional in character. This is probably because at lower pressures the stiffness of

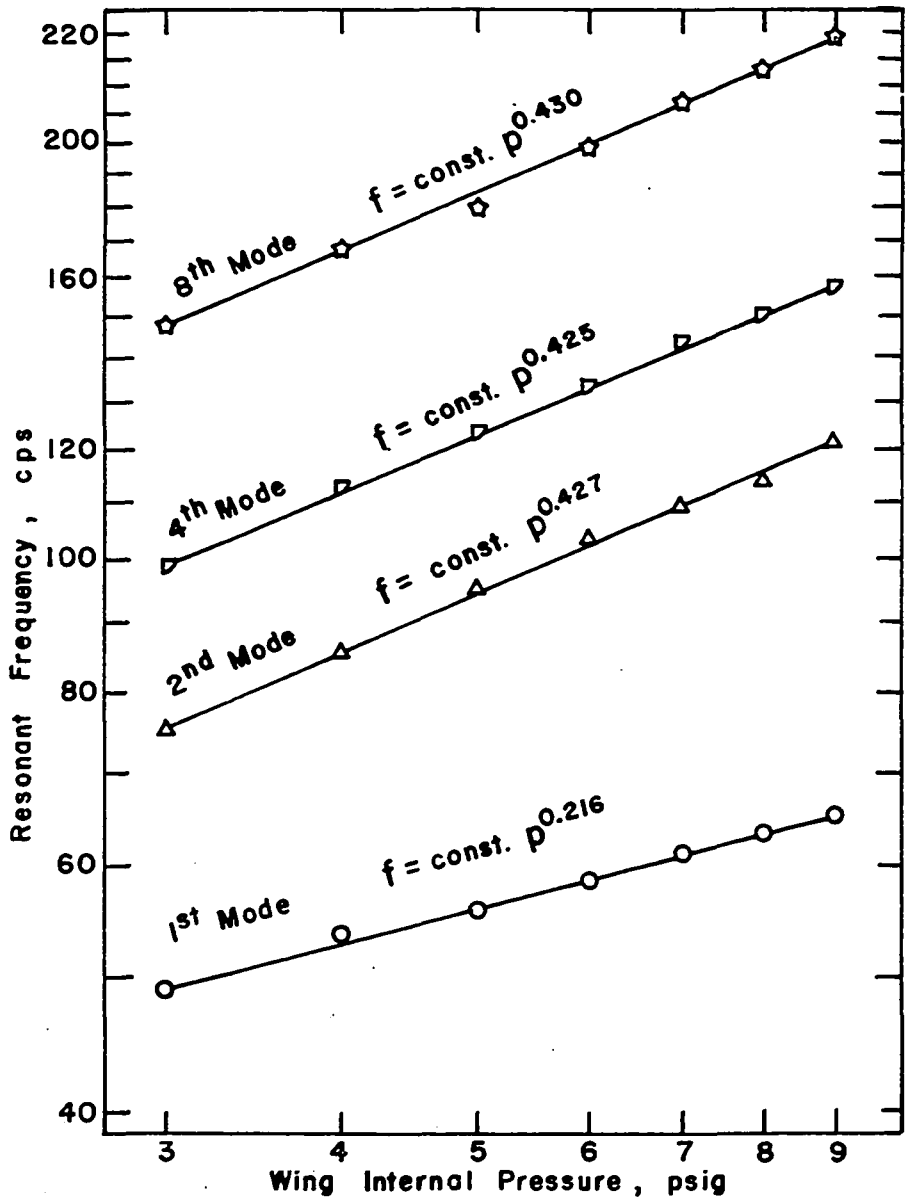

Figure 27. Log-log graph of experimental resonant frequencies of vibration excited with speaker shaker

the curved edge of the wing is a significant part of the total stiffness, but as the pressure is increased the edge stiffness becomes less and less important as compared to the shear stiffness due to the internal pressurized air. For the third mode the nodal line runs predominantly in a spanwise direction at three psig, but as the pressure is increased the nodal line swings around until, at nine psig it runs predominantly in a chordwise direction, indicating characteristics similar to those of a second bending mode of vibration. This is probably also a result of the decreasing importance of the edge stiffness. Examination of other nodal patterns reveals similar changes. Thus, as the internal pressure is increased, the edge effects become less and less important and the inflated wing acts more and more like a uniform plate.

2. Theoretical results

Application of the influence coefficient method, using ten sections, resulted in natural frequencies within four per cent of the experimental frequencies for the first (or fundamental) mode. The use of eighteen sections improved this to two per cent, thereby illustrating the increase in accuracy obtained by an increase in the number of sections. It should be noted here that the experimental values may be

incorrect by as much as one per cent because this was the limit of accuracy of the function generator used for exciting the wing model and indicating its resonant frequencies.

Difficulties were encountered in applying loads and measuring the deflections of a section when the center of gravity of the section fell on the curved portion of the edge of the model. This may have introduced errors, amount unknown, especially for the case of eighteen sections where the centers of gravity of ten of the sections fell on the curved edges. A more judicious arrangement of sections would cause fewer centers of gravity to fall on the edges.

The influence coefficient method using ten sections resulted in natural frequencies within 16 per cent of the experimental values for the second mode, 18 per cent for the third mode and 26 per cent for the fourth mode. The use of eighteen sections resulted in an eight per cent error for the second mode. Calculations of natural frequencies above the fundamental are increasingly less accurate because each sweeping process introduces a row of zeroes in the [D] matrix making the results dependent on fewer variables.

Influence coefficients were very accurately measured at 24 stations by Kordes *et al.* (16) and used by Kruszewski *et al.* (17) for finding the natural frequencies of a built-up 45-degree delta-wing. The results were below the experimental frequencies by 0.47 per cent for the first mode, 6.6

per cent for the second mode, four per cent for the third mode, and 11 per cent for the fourth mode.

Weidman and Kordes (39) measured influence coefficients at 29 stations on a multispan 60° delta wing and used these to calculate the natural frequencies of vibration. The results were below the experimental frequencies by nine per cent for the first mode, 2.7 per cent for the second mode and nine per cent for the third mode.

In the light of the above experiments with non-inflatable, delta wings, the author feels that the use of the influence coefficient method worked satisfactorily for finding the natural frequencies of vibration of the inflatable wing model. This is particularly true when one considers the possible increase in accuracy that would be obtained by the use of a larger number of sections, judiciously chosen.

3. Extension of results

It would be highly desirable to extend the results of the model tests to a full-sized prototype. The influence coefficient method does not appear to lend itself well to this type of procedure. It is often easier to use an analytic solution to extend results.

The use of an analytic solution for extending the

results of a model test to a full-sized prototype can be illustrated by looking at Stroud's (33) one term approximation of the solution to the problem of the vibration of a square, inflatable plate clamped on all four sides. He shows that for modes of vibration above the first, the natural frequency, $\omega \doteq \pi\sqrt{ph/\rho}\ (m^2/a + n^2/b)$, where p = the gauge pressure within the plate, h = thickness of the plate, ρ = the mass of plate per unit middle plane area, a and b are lengths of the plate in the transverse directions, and m and n are the number of half-waves in the transverse directions. This equation shows that the natural frequency varies inversely with the plates' transverse dimensions, directly with the square-root of the thickness of the plate, and inversely with the square-root of the unit mass of the plate. It is of interest to note that Stroud's equation as given above more closely resembles the equation for the natural frequency of vibration of a membrane than it does that for a solid plate, where the natural frequency is proportional to the inverse of the transverse dimensions squared.

B. Suggestions for Future Study

As has been suggested before, it would be desirable to have a theoretical solution to the problem of vibrations of an inflatable wing which could be used without resorting to

measured influence coefficients.

McComb (24) has developed a linear theory for inflatable plates in which the cover surfaces of the plate were treated as orthotropic membranes, the drop cords were assumed inextensional and conceptually spread continuously over the plate, and the sidewalls were presumed to be present at the edge of the plate, but to have no effect on the plate's behavior.

Appendix C presents McComb's equations and the boundary conditions appropriate to the cantilevered wing model. The assumptions made for the edges of the plate do not allow for the additional stiffness provided by the curved edges of the wing model under consideration here. Hence, the natural frequencies determined by the McComb method may not be in good agreement with the experimental results, especially at low internal pressures, where the edge stiffness contributes more to the overall wing stiffness. For a larger sized wing, such as might be used for an actual reentry vehicle, the effect of edge stiffness would be less important than it is for the model. Here the theory might fit better.

The solution of the McComb theory equations presented in Appendix C requires a numerical approach such as by finite differences. High-speed digital computing equipment will be needed for the application of this type of approach. The equations are included here for the aid of future

investigators who may wish to continue the work on the Goodyear wing model.

Another theoretical method of solving cantilever plate problems is that of Houbolt (13), who developed a set of difference equations for the bending of plates of variable thickness through the use of the energy equation. It is believed that his method will work for an inflatable plate and therefore an outline of his procedure is given here. Houbolt first divided the surface into a regular gridwork system. Then, by means of difference equations, he wrote the total potential energy of the system in terms of the deflection at each grid point, and then he minimized this energy expression with respect to each deflection point. Walton (38) applied Houbolt's method to the vibration of four cantilever solid plates of various shapes and found that the computed natural frequencies for the first five or six modes are accurate when compared with the experimental values. Use was made of high-speed computing equipment, which is essential for this method.

Appendix C gives the potential energy equation, as developed by McComb (24) for an inflatable plate.

VI. LITERATURE CITED

1. Anderson, S. L. A method for obtaining stress-strain relations in non-isotropic flexible sheet material under two-dimensional stress. Journal of Scientific Instruments 24: 25-27. 1947.

2. Anderson, William Judson. Vibration of a 60° delta wing model. Unpublished M.S. thesis. Ames, Iowa. Library, Iowa State University of Science and Technology. 1958.

3. Bisplinghoff, Raymond L., Ashley, Holt, and Halfman, Robert L. Aeroelasticity. Reading, Massachusetts. Addison-Wesley Publishing Company, Inc. 1955.

4. Fettis, Henry E. The calculations of coupled modes of vibration by the stodola method. Journal of the Aeronautical Sciences 16: 259-271. 1949.

5. Flomenhoft, H. I. A method for determining mode shapes and frequencies above the fundamental by matrix iteration. Journal of Applied Mechanics 17: 249-256. 1950.

6. Fung, Y. C. An introduction of the theory of aeroelasticity. New York, N.Y. John Wiley and Sons, Inc. 1955.

7. Gallacher, R. H. and Rattinger, I. The deformational behavior of low aspect ratio multi-web wings. Part I: Experimental data. The Aeronautical Quarterly 12: 361-371. 1961.

8. Gossard, Myron L. An iterative transformation procedure for numerical solution of flutter and similar characteristic-value problems. National Advisory Committee for Aeronautics Technical Note 2346. 1951.

9. Greenwood, Donald T. Some difference methods of plate vibration analysis. Thermofax. Ann Arbor, Michigan. Department of Aeronautical and Astronautical Engineering, University of Michigan. 1962.

10. Gustafson, P. N., Stokey, W. F., and Zorowski, C. F. An experimental study of natural vibrations of cantilevered triangular plates. Journal of the Aeronautical Sciences 20: 331-337. 1953.

11. Hedgepeth, John M. Recent research on the determination of natural modes and frequencies of aircraft wing structures. North Atlantic Treaty Organization, Advisory Committee for Aeronautical Research and Development Report 37. 1956.

12. Herr, Robert W. A wide-frequency-range air-jet shaker. National Advisory Committee for Aeronautics Technical Note 4060. 1957.

13. Houbolt, John C. A study of several aerothermoelastic problems of aircraft structures in high-speed flight. Zürich. Eidgenössischen Technischen Hochschule. Institut für Flugzeugstatik und Leichtbau Mitteilungen Nr. 5. 1958.

14. Hunt, Gerald L. and Walberg, Gerald D. Calculated mode shapes and pressure distributions at flutter for a highly tapered horizontal toil in subsonic flow. National Aeronautics and Space Administration Technical Note D-1008. 1962.

15. Kordes, Eldon E. and Kruszewski, Edwin T. Experimental investigation of the vibrations of a built-up rectangular box beam. National Advisory Committee for Aeronautics Technical Note 3618. 1956.

16. Kordes, Eldon E., Kruszewski, Edwin T., and Weidman, Deene J. Experimental influence coefficients and vibration modes of a built-up 45° delta-wing specimen. National Advisory Committee for Aeronautics Technical Note 3999. 1957.

17. Kruszewski, Edwin T., Kordes, Eldon E., and Weidman, Deene J. Theoretical and experimental investigations of delta-wing vibrations. National Advisory Committee for Aeronautics Technical Note 4015. 1957.

18. Leonard, R. W., McComb, H. G., Jr., Zender, G. W., and Stroud, W. J. Analysis of inflated reentry and space structures. Recovery of Space Vehicles Symposium. Proceedings. 1960: 62-78. 1960.

19. Leonard, Robert W. On the shear stiffness of fabrics. Journal of the Aerospace Sciences 29: 349-350. 1962.

20. Leonard, Robert W., Brooks, George W., and McComb, Harvey G., Jr. Structural considerations of inflatable reentry vehicles. National Aeronautics and Space Administration Technical Note D-457. 1960.

21. Levy, Samuel. Determination of influence coefficients. North Atlantic Treaty Organization, Advisory Committee for Aeronautical Research and Development Report 41. 1956.

22. Levy, Samuel. Structural analysis and influence coefficients for delta wings. Journal of the Aeronautical Sciences 20: 449-454. 1953.

23. Lewis, Robert C. and Wrisley, Donald L. A system for the excitation of pure natural modes of complex structures. Journal of the Aeronautical Sciences 17: 705-722. 1950.

24. McComb, Harvey G., Jr. A linear theory for inflatable plates of arbitrary shape. National Aeronautics and Space Administration Technical Note D-930. 1961.

25. McComb, Harvey G., Jr. and Leonard, Robert W. Slanted drop cords in inflatable airmat beams. [Multilithed] Langley Field, Virginia. Langley Research Center, National Aeronautics and Space Administration. 1961.

26. Minhinnick, I. T. The theoretical determination of normal modes and frequencies of vibration. North Atlantic Treaty Organization, Advisory Group for Aeronautical Research and Development Report 36. 1956.

27. Murphy, Glenn. Similitude in engineering. New York. The Ronald Press Company. 1950.

28. Myklestad, N. O. Fundamentals of vibration analysis. New York, N.Y. McGraw-Hill Book Company, Inc. 1956.

29. Reissner, Eric and Stein, Manuel. Torsion and transverse bending of cantilever plates. National Advisory Committee for Aeronautics Technical Note 2369. 1951.

30. Scanlan, Robert H. and Rosenbaum, Robert. Introduction to the study of aircraft vibration and flutter. New York, N.Y. The Macmillan Company. 1951.

31. Soroka, Walter W. Note on the relations between viscous and structural damping coefficients. Journal of the Aeronautical Sciences 16: 447-448. 1949.

32. Stein, Manuel and Sanders, J. Lyell, Jr. A method for deflection analysis of thin low-aspect-ratio wings. National Advisory Committee for Aeronautics Technical Note 3640. 1956.

33. Stroud, W. Jefferson. Experimental and theoretical deflections and natural frequencies of an inflatable plate. National Aeronautics and Space Administration Technical Note D-931. 1961.

34. Targoff, Walter P. The associated matrices of bending and coupled bending-torsion vibrations. Journal of the Aeronautical Sciences 14: 579-582. 1947.

35. Timoshenko, S. and Goodier, J. N. Theory of elasticity. New York, N.Y. McGraw-Hill Book Company, Inc. 1951.

36. Timoshenko, S. and Woinowsky-Krieger, S. Theory of plates and shells. New York, N.Y. McGraw-Hill Book Company, Inc. 1959.

37. Topping, A. D. An introduction to biaxial stress problems in fabric structures. Aerospace Engineering 20: 18-19. 1961.

38. Walton, William C., Jr. Applications of a general finite-difference method for calculating bending deformations of solid plates. National Aeronautics and Space Administration Technical Note D-536. 1960.

39. Weidman, Deene J. and Kordes, Eldon E. Experimental influence coefficients and vibration modes of a multi-span 60° delta wing. National Aeronautics and Space Administration Memorandum 2-4-59L. 1959.

40. Zender, George W. and Deaton, Jerry W. The stiffness properties of stressed fabrics as obtained from model tests. National Aeronautics and Space Administration Technical Note D-755. 1961.

VII. ACKNOWLEDGMENTS

The author wishes to thank Dr. E. W. Anderson for his guidance and encouragement during this study. He would also like to thank Goodyear Aircraft Corporation, Akron, Ohio, for furnishing the wing model and offering several helpful suggestions. In addition, he would like to thank his wife for her help in preparing the manuscript.

VIII. APPENDIX A: DERIVATION OF EQUATIONS

Consider the wing in Figure 28 as a thin elastic plate fixed at the root with the positive x (chordwise), y (spanwise), z (upward) directions as indicated. In accordance with a method described in Bisplinghoff (3) the transverse deflection under an inertial side load of intensity $-\rho(\nu,\eta)\, w(\nu,\eta,t)$ can be expressed in terms of the two-dimensional influence function as

$$w(x,y,t) = -\iint_S C(x,y;\nu,\eta)\, \rho(\nu,\eta)\, \ddot{w}(\nu,\eta,t)\, d\nu d\eta. \qquad \text{(Eq. 3)}$$

We now assume that the deflection of the continuous wing structure can be approximated by linear deflections at a finite number of discrete points. That is, the function $w(x,y,t)$ is approximated by a column matrix as follows:

$$w(x,y,t) = \begin{Bmatrix} w_1(t) \\ w_2(t) \\ w_3(t) \\ \vdots \\ w_n(t) \end{Bmatrix}, \qquad \text{(Eq. 4)}$$

where $w_i(t)$ represents the time dependent deflection of the i^{th} planform section of the subdivided wing as shown in Figure 28.

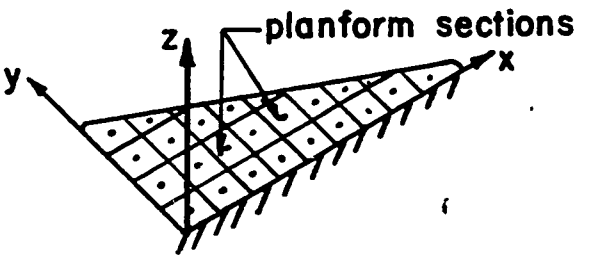

Figure 28. Wing divided into sections

The wing deflection at each of the n discrete points can be obtained from Equation 3 as

$$w_i(t) = - \iint_S C(x_i,y_i;\nu,\eta)\ \rho(\nu,\eta)\ \ddot{w}(\nu,\eta,t)\ d\nu d\eta,$$

$$(i = 1,2,3,\ldots,n). \qquad \text{(Eq. 5-6)}$$

If the wing mass (and hence the inertial force) is concentrated at the center of gravity of each section, Equation 5-6 can be approximated by a matrix equation:

$$\{w\} = - [C][M]\{\ddot{w}\}, \qquad \text{(Eq. 7-8)}$$

where [C] is a matrix of flexibility influence coefficients, [M] is a diagonal matrix of lumped section masses, and {w} is a column matrix as shown in Equation 4. Putting as a solution

$$w_i = W_i \cos(\omega t - \psi), \qquad \text{(Eq. 9-10)}$$

where W_i is the amplitude of the displacement w_i, ω is the frequency of oscillation, and ψ is the phase angle, we obtain from Equation 7-8

$$\{W\} = \omega^2[C][M]\{W\}. \qquad \text{(Eq. 11-12)}$$

Transposing the ω^2 we obtain

$$\frac{1}{\omega^2}\{W\} = [D]\{W\}, \qquad \text{(Eq. 13)}$$

where

$$[D] = [C][M]. \qquad \text{(Eq. 14)}$$

Equation 13 represents a set of characteristic equations that can be solved for values of ω^2 by matrix iteration as follows.

Let W_{1j}, where $j = 1,2,\ldots,n$, be an arbitrarily selected set of ordinates of the first mode. One of the W_{1j}'s, say W_{1n}, is set equal to 1. Substitution of this assumed modal column matrix into the right side of Equation 13 gives

$$[D]\{W_{1j}\} = \{N_{1j}\}. \qquad \text{(Eq. 15)}$$

Normalize the resulting column matrix, $\{N_{1j}\}$ by dividing by N_{1n}, so that the last element is again equal to 1:

$$\{N_{1j}\} = N_{1n}\{\frac{N_{1j}}{N_{1n}}\} = N_{1n}\{W_{2j}\}. \qquad \text{(Eq. 16)}$$

The process is repeated, this time using $\{W_{2j}\}$ as the approximation to the mode shape. If this iterative process is continued, successive values of the $\{W\}$ matrix will converge to the lowest natural mode, and the quantity $1/N_{mn}$ will converge to ω_1^2, when m becomes large. ω_1 is the lowest frequency of the system. Convergence is demonstrated by Blisplinghoff (3).

In order to find frequencies of vibration higher than the first and their respective mode shapes, the orthogonality condition between sets of ordinates can be used. (See Flomenhoft, 5) The orthogonality relation between the sets of ordinates of the first and second modes in the case of no dynamic coupling is

$$\sum_{i=1}^{n} B_i^{(1)} W_i^{(2)} = 0, \qquad \text{(Eq. 17)}$$

where

$$B_i^{(1)} = M_i W_i^{(1)}. \qquad \text{(Eq. 18)}$$

Solving for $W_1^{(2)}$:

$$W_1^{(2)} = -\frac{B_2^{(1)}}{B_1^{(1)}} W_2^{(2)} - \frac{B_3^{(1)}}{B_1^{(1)}} W_3^{(2)} - \cdots - \frac{B_n^{(1)}}{B_1^{(1)}} W_n^{(2)}. \qquad \text{(Eq. 19)}$$

Therefore, if W_2, W_3, ..., W_n are selected arbitrarily, W_1 is determined from Equation 19. In matrix form this can be written as

$$\begin{Bmatrix} W_1 \\ W_2 \\ \cdot \\ \cdot \\ \cdot \\ W_n \end{Bmatrix} = \begin{bmatrix} 0 & K_{12}^{(1)} & K_{13}^{(1)} & \cdots & K_{1n}^{(1)} \\ 0 & 1 & 0 & \cdots & 0 \\ \cdot & 0 & 1 & \cdots & 0 \\ \cdot & & & \cdot & \cdot \\ \cdot & & & \cdot & \cdot \\ 0 & 0 & 0 & \cdots & 1 \end{bmatrix} \begin{Bmatrix} W_1 \\ W_2 \\ \cdot \\ \cdot \\ \cdot \\ W_n \end{Bmatrix} \qquad \text{(Eq. 20)}$$

where

$$K_{1i}^{(1)} = -\frac{B_i^{(1)}}{B_1^{(1)}} \qquad \text{(Eq. 21)}$$

The square matrix in Equation 20 is called a "sweeping" matrix and designated $[S^{(1)}]$. If an arbitrary set of numbers W_1, W_2, ..., W_n is introduced into the right side of Equation 20, the product will yield a set of numbers W_1, W_2, ..., W_n which is orthogonal to the first mode. Therefore,

if the [D] matrix of Equation 13 is post-multiplied by the sweeping matrix $[S^{(1)}]$, the iteration process will then yield the second mode of vibration.

$$\frac{1}{\omega^2}\{W\} = [D][S^{(1)}]\{W\} = [D^{(1)}]\{W\}. \qquad \text{(Eq. 22)}$$

Equation 22, containing $[D^{(1)}]$, will converge to the second mode just as Equation 13, containing [D], converged to the first mode.

For finding the third mode two orthogonality conditions are known, and through the use of these, the new sweeping matrix $[S^{(2)}]$ can be found. Flomenhoft (5) gives a method whereby the sweeping matrix for the first mode $[S^{(1)}]$ is modified by an abbreviated sweeping matrix $[S^{(2)}]'$ to produce a sweeping matrix $[S^{(2)}]$ which will sweep the first two modes. A saving in effort is attained by modifying the previously swept $[D^{(1)}]$ matrix by $[S^{(2)}]'$, thus obtaining a matrix $[D^{(2)}]$ which is swept of both the first and second modes:

$$[D^{(2)}] = [D^{(1)}][S^{(2)}]', \qquad \text{(Eq. 23)}$$

where

$$[S^{(2)}]' = \begin{bmatrix} 1 & 0 & 0 & \cdot & \cdot & \cdot & 0 \\ 0 & 0 & K_{23}^{(2)} & K_{24}^{(2)} & \cdots & & K_{2n}^{(2)} \\ 0 & 0 & 1 & 0 & \cdots & & 0 \\ \cdot & \cdot & 0 & 1 & & & \cdot \\ \cdot & \cdot & & & \cdot & & \cdot \\ \cdot & \cdot & & & & \cdot & \cdot \\ 0 & 0 & \cdot & \cdot & \cdot & & 1 \end{bmatrix}, \qquad \text{(Eq. 24)}$$

$$K_{rj}^{(r)} = -\frac{\sum_{i=1}^{r-1} B_i^{(r)} K_{ij}^{(r-1)} + B_j^{(r)}}{\sum_{i=1}^{r-1} B_i^{(r)} K_{ir}^{(r-1)} + B_r^{(r)}}, \quad r+1 \leq j \leq n, \qquad \text{(Eq. 25)}$$

and

$$K_{ij}^{(r)} = K_{ir}^{(r-1)} K_{rj}^{(r)} + K_{ij}^{(r-1)}, \; i = 1 \text{ to } r-1, \; j = r+1 \text{ to } n. \qquad \text{(Eq. 26)}$$

The use of $[D^{(2)}]$ in place of $[D]$ in Equation 13 and the iteration process will produce the third mode.

For finding the fourth mode three orthogonality conditions are known and an abbreviated sweeping matrix $[S^{(3)}]'$ can be formed as follows:

$$[S^{(3)}]' = \begin{bmatrix} 1 & 0 & 0 & 0 & . & . & . & 0 \\ 0 & 1 & 0 & 0 & . & . & . & 0 \\ 0 & 0 & 0 & K_{34}^{(3)} & K_{35}^{(3)} & \cdots & & K_{3n}^{(3)} \\ . & 0 & 0 & 1 & 0 & \cdots & & 0 \\ . & . & . & & 1 & & & . \\ . & . & . & & & . & . & . \\ 0 & 0 & 0 & . & . & . & & 1 \end{bmatrix} \qquad \text{(Eq. 27)}$$

Therefore, when

$$[D^{(3)}] = [D^{(2)}][S^{(3)}]', \qquad \text{(Eq. 28)}$$

is used in place of [D] in Equation 13, iteration will produce convergence to the fourth mode.

IX. APPENDIX B: CALCULATIONS

$$[C] = \begin{bmatrix}
.026940, & .002610, & .008658, & .006345, & .003700, & .003628, & .001860, & .010540, & .007450, & .001928, \\
.002610, & .038400, & .001210, & .000907, & .002527, & .002420, & .000317, & .003518, & .004575, & .001360, \\
.008658, & .001210, & .020760, & .002438, & .001816, & .001755, & .002700, & .006492, & .004915, & .001210, \\
.006345, & .000907, & .002438, & .029560, & .000794, & .002246, & .002471, & .003176, & .001475, & .000408, \\
.003700, & .002527, & .001816, & .000794, & .017320, & .001816, & .000332, & .004785, & .005818, & .003233, \\
.003628, & .002420, & .001755, & .002246, & .001816, & .027300, & .000453, & .006650, & .003780, & .000846, \\
.001860, & .000317, & .002700, & .002471, & .000332, & .000453, & .019220, & .001316, & .000983, & .000347, \\
.010540, & .003518, & .006492, & .003176, & .004785, & .006650, & .001316, & .019400, & .009980, & .002308, \\
.007450, & .004575, & .004915, & .001475, & .005818, & .003780, & .000983, & .009980, & .009790, & .003343, \\
.001928, & .001360, & .001210, & .000408, & .003233, & .000846, & .000347, & .002308, & .003343, & .008200,
\end{bmatrix}$$

$$[M] = \begin{bmatrix}
.0002256 & & & & & & & & & \\
& .0001298 & & & & & & & & \\
& & .0003071 & & & & & & & \\
& & & .0001608 & & & & & & \\
& & & & .0002061 & & & & & \\
& & & & & .0001289 & & & & \\
& & & & & & .0002481 & & & \\
& & & & & & & .0001991 & & \\
& & & & & & & & .0001378 & \\
& & & & & & & & & .0002149
\end{bmatrix}$$

Figure 29. Influence coefficient and mass matrices for three psig internal wing pressure and ten subdivisions

A column matrix {W} was assumed and Equation 1 iterated with the following results.

Assumed

$$\{W\} = \begin{Bmatrix} 1.00000 \\ 1.00000 \\ 1.00000 \\ 1.00000 \\ 1.00000 \\ 1.00000 \\ 1.00000 \\ 1.00000 \\ 1.00000 \\ 1.00000 \end{Bmatrix},$$

First iteration,

$$\{W\} = \begin{Bmatrix} 3.33733 \\ 1.87808 \\ 2.69525 \\ 1.96855 \\ 1.78190 \\ 1.75613 \\ 1.53611 \\ 2.88350 \\ 2.17873 \\ 1.00000 \end{Bmatrix}, \quad . \quad . \quad . \quad ,$$

Seventh iteration,

$$\{W\} = \begin{Bmatrix} 5.68073 \\ 1.92119 \\ 4.39201 \\ 2.50730 \\ 2.02914 \\ 2.13344 \\ 1.34120 \\ 4.37581 \\ 3.06768 \\ 1.00000 \end{Bmatrix},$$

Eigth iteration

$$\{W\} = \begin{Bmatrix} 5.68377 \\ 1.91749 \\ 4.39539 \\ 2.50713 \\ 2.02889 \\ 2.13321 \\ 1.33964 \\ 4.37717 \\ 3.06834 \\ 1.00000 \end{Bmatrix},$$

$(1/\omega)^2 = 45.9251_{D}\text{-}07, \quad . \quad . \quad . \quad , \quad (1/\omega)^2 = 11.4865_{D}\text{-}06, \quad (1/\omega)^2 = 11.4929_{D}\text{-}06,$

$f = 74.2669 \text{ cps}, \quad . \quad . \quad . \quad , \quad f = 46.9599 \text{ cps}, \quad f = 46.9469 \text{ cps}.$

Figure 30. Iteration procedure for first mode of vibration for three psig internal wing pressure and ten subdivisions

The second, third and fourth modes are found as described in appendix A. The results of the iterations are:

Second mode
21 iterations

$$\{W\} = \begin{Bmatrix} -1.07743 \\ 11.23324 \\ -3.25912 \\ -1.51182 \\ 2.60853 \\ 2.23207 \\ -1.01627 \\ 1.43850 \\ 1.77475 \\ 1.00000 \end{Bmatrix},$$

$f = 68.8791$ cps,

Third mode
27 iterations

$$\{W\} = \begin{Bmatrix} 3.85405 \\ -6.08402 \\ -3.09727 \\ -3.39438 \\ 3.28221 \\ 3.00234 \\ -12.64024 \\ 3.51446 \\ 2.02262 \\ 1.00000 \end{Bmatrix},$$

$f = 72.1713$ cps[a],

Fourth mode
37 iterations

$$\{W\} = \begin{Bmatrix} -16.62894 \\ 11.66881 \\ 37.11931 \\ -63.06044 \\ 0.19608 \\ -11.00775 \\ -10.02320 \\ -1.57741 \\ 2.83712 \\ 1.00000 \end{Bmatrix},$$

$f = 72.1555$ cps[a].

[a] Because only ten sections were used, the results for the third and fourth modes are not accurate.

Figure 31. Second, third and fourth mode iteration results for three psig internal wing pressure and ten subdivisions

$$[C] = \begin{bmatrix}
.020760, & .002040, & .006845, & .004218, & .002620, & .002584, & .001810, & .007110, & .006185, & .001424, \\
.002040, & .020920, & .000977, & .000907, & .002268, & .001677, & .000208, & .002970, & .003716, & .001087, \\
.006845, & .000977, & .013280, & .002020, & .001550, & .001450, & .002500, & .005250, & .003830, & .001054, \\
.004218, & .000907, & .002020, & .018370, & .000770, & .001971, & .001950, & .002472, & .001814, & .000326, \\
.002620, & .002268, & .001550, & .000770, & .011300, & .001360, & .000235, & .003380, & .004390, & .002220, \\
.002584, & .001677, & .001450, & .001971, & .001360, & .015500, & .000399, & .004530, & .003130, & .000689, \\
.001810, & .000208, & .002500, & .001950, & .000235, & .000399, & .010650, & .001270, & .000843, & .000215, \\
.007110, & .002970, & .005250, & .002472, & .003380, & .004530, & .001270, & .015750, & .007310, & .002040, \\
.006185, & .003716, & .003830, & .001814, & .004390, & .003130, & .000843, & .007310, & .007070, & .002268, \\
.001424, & .001087, & .001054, & .000326, & .002220, & .000689, & .000215, & .002040, & .002268, & .005710,
\end{bmatrix}$$

$$[M] = \begin{bmatrix}
.0002268 & & & & & & & & & \\
& .0001307 & & & & & & & & \\
& & .0003084 & & & & & & & \\
& & & .0001620 & & & & & & \\
& & & & .0002071 & & & & & \\
& & & & & .0001298 & & & & \\
& & & & & & .0002494 & & & \\
& & & & & & & .0002002 & & \\
& & & & & & & & .0001384 & \\
& & & & & & & & & .0002156
\end{bmatrix}$$

Figure 32. Influence coefficient and mass matrices for five psig internal wing pressure and ten subdivisions

The results of the iterations are:

First mode 8 iterations	Second mode 23 iterations	Third mode 30 iterations	Fourth mode 31 iterations
$\{W\} = \begin{Bmatrix} 5.64543 \\ 1.70053 \\ 4.00358 \\ 2.23606 \\ 1.88813 \\ 1.87219 \\ 1.32739 \\ 4.34693 \\ 3.12340 \\ 1.00000 \end{Bmatrix}$,	$\{W\} = \begin{Bmatrix} -1.10528 \\ 4.26134 \\ -2.04986 \\ -1.24329 \\ 2.56473 \\ 1.68856 \\ -1.93461 \\ 2.01961 \\ 1.62347 \\ 1.00000 \end{Bmatrix}$,	$\{W\} = \begin{Bmatrix} -14.85676 \\ 9.06236 \\ 7.01551 \\ 2.32254 \\ 1.74169 \\ 1.52249 \\ 13.34567 \\ 1.84755 \\ 0.48209 \\ 1.00000 \end{Bmatrix}$,	$\{W\} = \begin{Bmatrix} -1.48874 \\ -4.09756 \\ 9.95080 \\ -26.60103 \\ 1.03823 \\ -4.29292 \\ -4.33660 \\ 1.94800 \\ 0.76749 \\ 1.00000 \end{Bmatrix}$,
$f = 54.3440$ cps,	$f = 87.5101$ cps,	$f = 96.5654$ cps[a],	$f = 93.6252$ cps[a].

[a] Because only ten sections were used, the results for the third and fourth modes are not accurate.

Figure 33. Iteration results for five psig internal wing pressure and ten subdivisions

$$[C] = \begin{bmatrix}
.016000, & .001768, & .006070, & .003435, & .002170, & .002140, & .001473, & .007092, & .004880, & .000905, \\
.001768, & .015880, & .000922, & .000680, & .002051, & .001473, & .000186, & .002378, & .003185, & .000915, \\
.006070, & .000922, & .012270, & .001738, & .001029, & .001064, & .002355, & .004310, & .002742, & .000741, \\
.003435, & .000680, & .001738, & .013300, & .000485, & .001746, & .001268, & .002246, & .001269, & .000253, \\
.002170, & .002051, & .001029, & .000485, & .008790, & .000879, & .000254, & .002914, & .003790, & .002460, \\
.002140, & .001473, & .001064, & .001746, & .000879, & .012610, & .000295, & .003840, & .002170, & .000553, \\
.001473, & .000186, & .002335, & .001268, & .000254, & .000295, & .009200, & .001020, & .000652, & .000185, \\
.007092, & .002378, & .004310, & .002246, & .002914, & .003840, & .001020, & .012520, & .006380, & .001384, \\
.004880, & .003185, & .002742, & .001269, & .003790, & .002170, & .000652, & .006380, & .006885, & .002412, \\
.000905, & .000915, & .000741, & .000253, & .002460, & .000553, & .000185, & .001384, & .002412, & .004980,
\end{bmatrix}$$

$$[M] = \begin{bmatrix}
.0002280 & & & & & & & & & \\
& .0001316 & & & & & & & & \\
& & .0003097 & & & & & & & \\
& & & .0001631 & & & & & & \\
& & & & .0002082 & & & & & \\
& & & & & .0001307 & & & & \\
& & & & & & .0002507 & & & \\
& & & & & & & .0002013 & & \\
& & & & & & & & .0001390 & \\
& & & & & & & & & .0002163
\end{bmatrix}$$

Figure 34. Influence coefficient and mass matrices for seven psig internal wing pressure and ten subdivisions

The results of the iterations are:

First mode
8 iterations

$$\{W\} = \begin{Bmatrix} 5.92528 \\ 1.76122 \\ 4.63264 \\ 2.18728 \\ 1.91371 \\ 1.89042 \\ 1.47867 \\ 4.78914 \\ 3.26944 \\ 1.00000 \end{Bmatrix},$$

$f = 58.9904$ cps,

Second mode
28 iterations

$$\{W\} = \begin{Bmatrix} 0.12994 \\ 2.52533 \\ -2.70325 \\ -0.07211 \\ 2.12553 \\ 1.42458 \\ -1.83605 \\ 1.69594 \\ 1.70357 \\ 1.00000 \end{Bmatrix},$$

$f = 92.9243$ cps,

Third mode
20 iterations

$$\{W\} = \begin{Bmatrix} -2.53441 \\ 2.92286 \\ 0.78143 \\ -1.26507 \\ 1.69637 \\ -0.05897 \\ 2.86232 \\ -0.19567 \\ 0.69809 \\ 1.00000 \end{Bmatrix},$$

$f = 107.0071$ cps[a],

Fourth mode
31 iterations

$$\{W\} = \begin{Bmatrix} -0.38064 \\ 0.02781 \\ 4.30759 \\ -11.31804 \\ 1.68119 \\ -3.08090 \\ -6.11796 \\ 0.15333 \\ 0.84945 \\ 1.00000 \end{Bmatrix},$$

$f = 107.6053$ cps[a],

[a] Because only ten sections were used, the results for the third and fourth modes are not accurate.

Figure 35. Iteration results for seven psig internal wing pressure and ten subdivisions

$$[C] = \begin{bmatrix}
.014330, & .001224, & .005600, & .002835, & .001663, & .001916, & .001402, & .006185, & .004600, & .000815, \\
.001224, & .011160, & .000725, & .000512, & .001496, & .001125, & .000258, & .001893, & .002844, & .000838, \\
.005600, & .000725, & .010610, & .001349, & .000838, & .000907, & .002142, & .003585, & .002337, & .000421, \\
.002835, & .000512, & .001349, & .010200, & .000398, & .001180, & .001270, & .002156, & .001303, & .000313, \\
.001663, & .001496, & .000838, & .000398, & .006750, & .000752, & .000274, & .002222, & .003230, & .001925, \\
.001916, & .001125, & .000907, & .001180, & .000725, & .009200, & .000470, & .002587, & .002154, & .000353, \\
.001402, & .000258, & .002142, & .001270, & .000274, & .000470, & .007660, & .000809, & .000630, & .000126, \\
.006185, & .001893, & .003585, & .002156, & .002222, & .002587, & .000809, & .010390, & .004780, & .001731, \\
.004600, & .002844, & .002337, & .001303, & .003230, & .002154, & .000630, & .004780, & .005710, & .001731, \\
.000815, & .000838, & .000421, & .000313, & .001925, & .000353, & .000126, & .001731, & .001731, & .004580,
\end{bmatrix}$$

$$[M] = \begin{bmatrix}
.0002292 & & & & & & & & & \\
& .0001325 & & & & & & & & \\
& & .0003110 & & & & & & & \\
& & & .0001643 & & & & & & \\
& & & & .0002093 & & & & & \\
& & & & & .0001316 & & & & \\
& & & & & & .0002520 & & & \\
& & & & & & & .0002023 & & \\
& & & & & & & & .0001396 & \\
& & & & & & & & & .0002170
\end{bmatrix}$$

Figure 36. Influence coefficient and mass matrices for nine psig internal wing pressure and ten subdivisions

The results of the iterations are:

First mode
8 iterations

$$\{W\} = \begin{Bmatrix} 6.35656 \\ 1.48598 \\ 4.84206 \\ 2.12255 \\ 1.70393 \\ 1.70908 \\ 1.60034 \\ 4.67715 \\ 3.25673 \\ 1.00000 \end{Bmatrix},$$

$f = 63.2634$ cps ,

Second mode
32 iterations

$$\{W\} = \begin{Bmatrix} 0.34545 \\ 1.52445 \\ -2.24904 \\ 0.25926 \\ 1.54763 \\ 0.94766 \\ -1.41069 \\ 1.52483 \\ 1.39865 \\ 1.00000 \end{Bmatrix},$$

$f = 101.8771$ cps ,

Third mode
19 iterations

$$\{W\} = \begin{Bmatrix} -2.43023 \\ 2.18936 \\ 0.18140 \\ 0.51191 \\ 1.61076 \\ 0.61608 \\ 3.21489 \\ 0.10190 \\ 0.73662 \\ 1.00000 \end{Bmatrix},$$

$f = 117.6864$ cps [a] ,

Fourth mode
22 iterations

$$\{W\} = \begin{Bmatrix} -1.90958 \\ 2.19442 \\ 2.70676 \\ -5.03494 \\ 1.74028 \\ -0.70978 \\ -2.67198 \\ 0.09449 \\ 0.75205 \\ 1.00000 \end{Bmatrix},$$

$f = 119.0891$ cps [a] .

[a] Because only ten sections were used, the results for the third and fourth modes are not accurate.

Figure 37. Iteration results for nine psig internal wing pressure and ten subdivisions

Figure 38. Influence coefficient matrix for seven psig internal wing pressure and eighteen subdivisions

$$[C] = \begin{bmatrix}
.013068, .002625, .007930, .003176, .001550, .004080, .005442, .004425, .006345, .005210, \\
.000408, .001133, .002381, .003960, .002391, .001816, .007140, .001315, \\
.002625, .014560, .001927, .000770, .000340, .000959, .001270, .000816, .003060, .003851, \\
.000110, .000220, .000317, .001543, .001270, .001928, .001497, .002190, \\
.007930, .001927, .009966, .003855, .002268, .005320, .000623, .006800, .005890, .004870, \\
.001836, .001058, .002042, .002834, .002040, .001360, .009740, .001248, \\
.003176, .000770, .003855, .007975, .003627, .003855, .002720, .005890, .002268, .001588, \\
.001564, .001058, .007040, .000952, .000612, .000407, .005210, .000408, \\
.001550, .000340, .002268, .003627, .004730, .002494, .001592, .003515, .001057, .000816, \\
.001473, .001360, .000498, .000498, .000226, .000272, .002947, .000265, \\
.004080, .000959, .005320, .003855, .002494, .025000, .006322, .005100, .003173, .002041, \\
.001190, .004530, .003060, .001588, .000861, .000589, .005890, .000479, \\
.005442, .001270, .000623, .002720, .001592, .006322, .023600, .003627, .004082, .003176, \\
.000589, .002268, .005780, .003510, .001361, .000907, .005665, .000816, \\
.004425, .000816, .006800, .005890, .003515, .005100, .003627, .009520, .003400, .001700, \\
.001360, .001020, .001133, .001521, .000907, .000634, .007705, .000544, \\
.006345, .003060, .005890, .002268, .001057, .003173, .004082, .003400, .009878, .005435, \\
.000317, .000702, .001315, .002948, .003286, .002154, .004875, .001700, \\
.005210, .003851, .004870, .001588, .000816, .002041, .003176, .001700, .005435, .006490, \\
.000271, .000498, .000861, .001928, .002268, .002836, .003855, .002495, \\
.000408, .000110, .001836, .001564, .001473, .001190, .000589, .001360, .000317, .000271, \\
.002488, .000891, .000202, .000172, .000110, .000077, .000951, .000097, \\
.001133, .000220, .001058, .001058, .001360, .004530, .002268, .001020, .000702, .000498, \\
.000891, .021300, .002155, .000695, .000285, .000136, .001360, .000110, \\
.002381, .000317, .002042, .007040, .000498, .003060, .005780, .001133, .001315, .000861, \\
.000202, .002155, .016800, .002268, .000543, .000408, .001566, .000233, \\
.003960, .001544, .002834, .000952, .000498, .001588, .003510, .001521, .002948, .001928, \\
.000172, .000695, .002268, .014520, .002382, .000815, .002222, .000453, \\
.002391, .001270, .002040, .000612, .000226, .000861, .001361, .000907, .003286, .002268, \\
.000110, .000285, .000543, .002382, .015400, .001813, .001360, .000679, \\
.001816, .001928, .001360, .000407, .000272, .000589, .000907, .000634, .002154, .002836, \\
.000077, .000136, .000408, .000815, .001813, .015000, .000951, .001043, \\
.007140, .001497, .009740, .005210, .002947, .005890, .005665, .007705, .004875, .003855, \\
.000951, .001360, .001566, .002222, .001360, .000951, .011460, .000951, \\
.001315, .002190, .001248, .000408, .000265, .000479, .000816, .000544, .001700, .002495, \\
.000097, .000110, .000233, .000453, .000679, .001043, .000951, .002488,
\end{bmatrix}$$

$$[M] = \begin{bmatrix} .0001239 & & & & & & & & & & & & & & & & & \\ & .0001364 & & & & & & & & & & & & & & & & \\ & & .0001101 & & & & & & & & & & & & & & & \\ & & & .0000917 & & & & & & & & & & & & & & \\ & & & & .0001048 & & & & & & & & & & & & & \\ & & & & & .0001262 & & & & & & & & & & & & \\ & & & & & & .0000916 & & & & & & & & & & & \\ & & & & & & & .0001093 & & & & & & & & & & \\ & & & & & & & & .0001258 & & & & & & & & & \\ & & & & & & & & & .0001017 & & & & & & & & \\ & & & & & & & & & & .0001034 & & & & & & & \\ & & & & & & & & & & & .0001176 & & & & & & \\ & & & & & & & & & & & & .0001047 & & & & & \\ & & & & & & & & & & & & & .0001145 & & & & \\ & & & & & & & & & & & & & & .0001047 & & & \\ & & & & & & & & & & & & & & & .0000916 & & \\ & & & & & & & & & & & & & & & & .0001217 & \\ & & & & & & & & & & & & & & & & & .0001177 \end{bmatrix}$$

Figure 39. Mass matrix for seven psig internal wing pressure and eighteen subdivisions

The results of the iterations are:

First mode, 7 iterations.

$$\{W\} = \begin{Bmatrix} 4.17591 \\ 1.99386 \\ 3.88175 \\ 2.58860 \\ 1.46637 \\ 2.85027 \\ 3.63603 \\ 3.14012 \\ 3.36263 \\ 2.67779 \\ 0.75583 \\ 1.53300 \\ 2.22338 \\ 2.34590 \\ 1.78486 \\ 1.39507 \\ 4.10517 \\ 1.00000 \end{Bmatrix},$$

$f = 62.6446$ cps,

Second mode, 29 iterations.

$$\{W\} = \begin{Bmatrix} 0.15412 \\ 3.40683 \\ 0.90152 \\ -0.61823 \\ -0.12551 \\ -1.15965 \\ -2.16556 \\ 0.11581 \\ 1.46705 \\ 1.55814 \\ 0.05572 \\ -5.43285 \\ -2.24048 \\ 0.62642 \\ 1.96968 \\ 1.95498 \\ 0.19410 \\ 1.00000 \end{Bmatrix},$$

$f = 100.0206$ cps.

Figure 40. Iteration results for seven psig internal wing pressure and eighteen subdivisions

X. APPENDIX C: INFLATABLE PLATE EQUATIONS

A. Differential Equations

The equations developed by McComb (24) as applied to a freely vibrating inflatable plate of constant thickness, h, where in-plane accelerations are neglected, become

$$ph\left(\frac{\partial \alpha}{\partial x} + \frac{\partial^2 w}{\partial x^2} + \frac{\partial \beta}{\partial y} + \frac{\partial^2 w}{\partial y^2}\right) = \rho \ddot{w},$$

$$\frac{\partial M_x}{\partial x} + \frac{\partial M_{xy}}{\partial y} - ph\left(\alpha + \frac{\partial w}{\partial x}\right) = \frac{h^2}{4} \rho \ddot{\alpha},$$

$$\frac{\partial M_y}{\partial y} + \frac{\partial M_{xy}}{\partial x} - ph\left(\beta + \frac{\partial w}{\partial y}\right) = \frac{h^2}{4} \rho \ddot{\beta}, \qquad \text{(Eq. 29)}$$

where w is the displacement of the plate in the z- (or transverse) direction, α and β are the angles of rotation of the drop cords in the zx- and yz-planes, respectively, from their initial position normal to the xy-plane, and M_x, M_y and M_{xy} are the plate moment resultants, positive as shown in Figure 41.

The boundary conditions applicable to the problem of the cantilevered wing model clamped along the x-axis as shown in Figure 41 are:

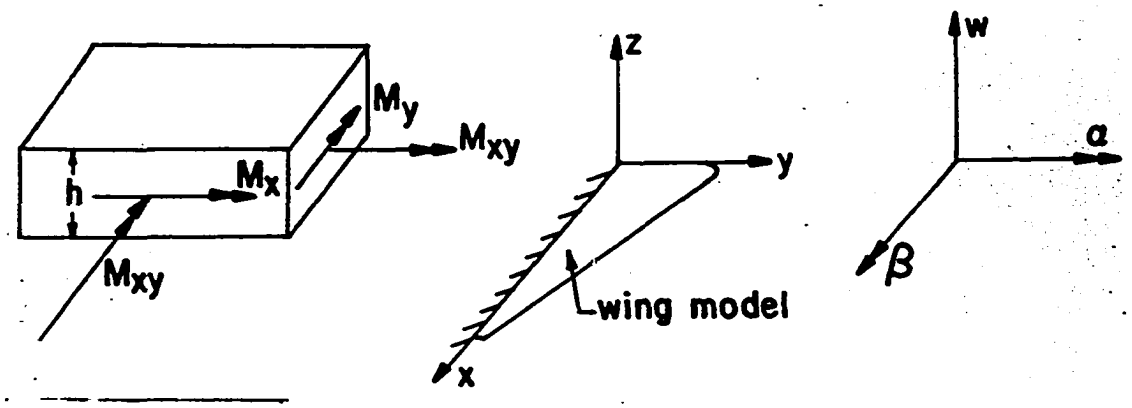

Figure 41. Sign conventions

$w(x,0) = \alpha(x,0) = \beta(x,0) = 0$, along the clamped edge;

$$ph(\alpha + \frac{\partial w}{\partial x}) = 0, \text{ along a free edge perpendicular to x-axis;}$$

$$M_x - \frac{ph^3}{12}\frac{\partial \beta}{\partial y} = 0, \text{ along a free edge perpendicular to x-axis;}$$

$$M_{xy} + \frac{ph^3}{12}\frac{\partial \alpha}{\partial y} = 0, \text{ along a free edge perpendicular to x-axis;}$$

$$ph(\beta + \frac{\partial w}{\partial y}) = 0, \text{ along a free edge perpendicular to y-axis;}$$

$$M_{xy} + \frac{ph^3}{12}\frac{\partial \beta}{\partial x} = 0, \text{ along a free edge perpendicular to y-axis;}$$

$$M_y - \frac{ph^3}{12}\frac{\partial \alpha}{\partial x} = 0, \text{ along a free edge perpendicular to y-axis.}$$

(Eq. 30)

The moments can be expressed in terms of w, α, and β as

$$M_x = \frac{h^2}{2}\left(A_{11}\frac{\partial\alpha}{\partial x} + A_{12}\frac{\partial\beta}{\partial y}\right),$$

$$M_y = \frac{h^2}{2}\left(A_{21}\frac{\partial\alpha}{\partial x} + A_{22}\frac{\partial\beta}{\partial y}\right),$$

$$M_{xy} = \frac{h^2}{2}A_{33}\left(\frac{\partial\alpha}{\partial y} + \frac{\partial\beta}{\partial x}\right),$$

where

$$A_{11} = \frac{E_W t}{1 - \mu_{WF}\mu_{FW}}, \quad A_{12} = \frac{\mu_{FW}E_W t}{1 - \mu_{WF}\mu_{FW}},$$

$$A_{22} = \frac{E_F t}{1 - \mu_{WF}\mu_{FW}}, \quad A_{21} = \frac{\mu_{WF}E_F t}{1 - \mu_{WF}\mu_{FW}}$$

$$A_{33} = Gt. \qquad \text{(Eq. 31)}$$

The subscripts W and F refer to the warp and fill directions, respectively, of the fabric material. The x- and y-directions are aligned with the warp and fill directions, respectively.

B. Energy Equation

The potential energy for small deflections of an inflatable plate for which there are no edge loads or moments

and the transverse displacements are not specified on the boundaries is given by McComb (24) as

$$U = \iint \{\tfrac{1}{2}ph[(\frac{\partial w}{\partial x})^2 + (\frac{\partial w}{\partial y})^2] + \frac{h^2}{4}[A_{11}(\frac{\partial \alpha}{\partial x})^2 + A_{22}(\frac{\partial \beta}{\partial y})^2$$

$$+ 2A_{12}\frac{\partial \alpha}{\partial x}\frac{\partial \beta}{\partial y} + A_{33}(\frac{\partial \alpha}{\partial y} + \frac{\partial \beta}{\partial x})^2] + ph[\frac{\alpha^2}{2} + \frac{\beta^2}{2} + \alpha\frac{\partial w}{\partial x}$$

$$+ \beta\frac{\partial w}{\partial y} - \frac{h^2}{12}(\frac{\partial \alpha}{\partial x}\frac{\partial \beta}{\partial y} - \frac{\partial \alpha}{\partial y}\frac{\partial \beta}{\partial x})] - qw\}\, dxdy, \qquad \text{(Eq. 32)}$$

where q is the transverse (z-direction) distributed load per unit area.

The finite difference expressions can be of the following type:

$$[\frac{\partial \varphi}{\partial x}]_{i,j} \doteq \frac{1}{2\epsilon}(\varphi_{i-1,j} - \varphi_{i+1,j}),$$

$$[\frac{\partial \varphi}{\partial y}]_{i,j} \doteq \frac{1}{2\lambda}(\varphi_{i,j-1} - \varphi_{i,j+1}),$$

where φ represents either w, α, or β, and ϵ and λ are the intervals between grid lines in the x- and y-directions, respectively, as shown in Figure 42.

In order to effect a solution the energy equation might be expressed in finite difference form for each of the grid

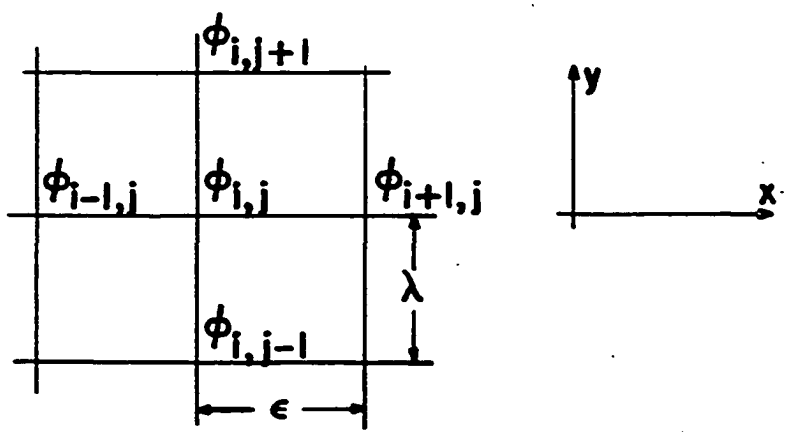

Figure 42. Grid points and intervals

points in terms of the unknown deflections and rotations at grid points in the vicinity of the point of evaluation. Then the integration of 32 might be evaluated by integration of the trapezoidal type to get an approximate expression for the energy, in terms of the unknown deflections and rotations of the grid points. Next use is made of the principle of minimum potential energy which requires that

$$\frac{\partial U}{\partial \varphi_{i,j}} = 0, \text{ (for each grid point i,j),} \qquad \text{(Eq. 33)}$$

where $\varphi_{i,j}$ is w, α, and β in turn.

Equation 33 represents a set of simultaneous equations which can be solved for the unknown deflections and rotations at each of the grid points.